cellular matrix signaling pathways for cell cycle and cell proliferation (28), and increase of expression of podoplanin is also related to tumor malignancy and poor clinical outcome (22, 29, 30).

To establish targeted therapy to podoplanin, we previously generated a rat anti-human podoplanin mAb NZ-1 (31, 32). NZ-1 suppressed podoplanin-induced pulmonary metastasis by inhibiting tumor-induced platelet aggregation (27). Furthermore, we showed that NZ-1 has not only high specificity and sensitivity but also high binding affinity against podoplanin, leading to its status as a candidate for radioimmunotherapy or immunotoxin therapy (33). However, it has not been clarified whether NZ-1 has antitumor effector functions including Ab-dependent cellular cytotoxicity (ADCC) and complement-dependent cytotoxicity (CDC), which is the most important mechanism contributing to the clinical efficacy of therapeutic Abs (34).

In the current study, we investigated whether NZ-1 can induce antitumor effects mediated by ADCC and CDC against MPM in vitro and in vivo. Furthermore, we also evaluated antitumor activity of NZ-8, a novel rat-human chimeric anti-human podoplanin Ab, using human mononuclear cells (MNC) as effector cells against MPM cells.

Materials and Methods

Cell lines

In this study, we used 15 human MPM cell lines. ACC-MESO-1, ACC-MESO-4, Y-MESO-8A, Y-MESO-9, Y-MESO-12, and Y-MESO-14 were established in Aichi Cancer Research Center Institute (35). EHMES-1 was provided by Dr. Hironobu Hamada (Ehime University, Matsuyama, Japan) (36). NCI-H290 and NCI-H513 were provided by Dr. Adi F. Gazdar (University of Texas Southwestern Medical Center, Dallas, TX). MSTO-211H, NCI-H28, NCI-H226, NCI-H2052, NCI-H2373, NCI-H2452, and Chinese hamster ovary (CHO) were purchased from American Type Culture Collection (Rockville, MD). MPM cell lines are divided into three histological origins, an epithelioid type (ACC-MESO-1, ACC-MESO-4, Y-MESO-9, Y-MESO-12, NCI-H290, NCI-H513, NCI-H226, and NCI-H2452), a sarcomatoid type (NCI-H28, NCI-H2052, and NCI-H2373), and a biphasic type (Y-MESO-8A, Y-MESO-14, EHMES-1, and MSTO-211H) (37–39). These cells were cultured in RPMI 1640 medium supplemented with 10% FBS (CRPMI 1640; Life Technologies, Grand Island, NY), 100 U/ml penicillin, and 100 μg/ml streptomycin (Meiji Seika Kaisha, Tokyo, Japan). Cell lines were authenticated by DNA fingerprinting. MSTO-211H cells were transfected with appropriate amounts of plasmids, pcDNA3/human podoplanin (PDPN) or pcDNA3/mock (11), using Metafectene (Nippon Genetics, Tokyo, Japan) according to the manufacturer's instructions. Stable transfectants (MSTO-211H/PDPN and MSTO-211H/mock) were selected by cultivating the transfectants in medium containing 0.5 mg/ml Geneticin (Invitrogen, Carlsbad, CA).

Abs

NZ-1, a rat anti-human podoplanin mAb (IgG_{2a}), was developed as described previously (31). Rat IgG and human IgG were purchased from Beckman Coulter (Fullerton, CA). For the generation of rat-human chimera anti-human podoplanin (NZ-8), the appropriate V_H and V_L cDNAs of a rat NZ-1 Ab and C_H and C_L of human IgG_1 were subcloned into the pcDNA3.3/Neo or pcDNA3.1/Zeo vectors (Life Technologies), respectively. The cDNAs coding for the V_H and V_L (κ-chain) regions were constructed by a PCR-based method. Ab expression vectors were transfected into CHO cells using Lipofectamine 2000 reagent (Life Technologies). Stable transfectants of CHO/NZ-8 were selected by cultivating the transfectants in medium containing 1 mg/ml Geneticin and 0.5 mg/ml Zeocin (Life Technologies). CHO/NZ-8 cells were cultivated in CHO-S-SFM II medium (Life Technologies). The media containing NZ-8 were centrifuged, and the obtained supernatant was applied to a column of protein G-Sepharose (Thermo Scientific, Rockford, IL). After extensive washing with PBS, the fusion proteins were eluted using 0.1 M glycine and 0.15 M NaCl (pH 2.8) and then neutralized with 1 M Tris (pH 10). The Abs were dialyzed against PBS. Expression and purity of the proteins were confirmed by SDS-PAGE using 5–20% gradient gels (Wako Pure Chemical Industries, Osaka, Japan). $F(ab')_2$ fragments of NZ-1 Ab were prepared using $F(ab')_2$ Preparation Kits (Thermo Scientific) according to the manufacturer's instructions. D2-40 (mouse anti-human podoplanin mAb) was purchased from DakoCytomation (Glostrup, Denmark).

Animals

Male SCID mice, 5 to 6 wk old, and male Wistar rats, 6 wk old, were obtained from CLEA Japan (Osaka, Japan) and maintained under specific pathogen-free conditions throughout this study. All animals were acclimatized for at least 1 wk before experiments. All experiments were performed in accordance with the guidelines of University of Tokushima, Committee on Animal Care and Use.

Flow cytometry

Expression of podoplanin was detected by flow cytometry. Cells (5×10^5) were washed with cold PBS and stained on ice for 30 min with NZ-1 (1 μg/ml), NZ-1 $F(ab')_2$ fragment (0.675 μg/ml), NZ-8 (1 μg/ml), rat IgG (1 μg/ml), or human IgG (1 μg/ml). After incubation with the primary mAbs, cells were washed with cold PBS and then incubated on ice for 30 min with FITC-conjugated goat $F(ab')_2$ fragment anti-rat IgG (H+L) Ab or FITC-conjugated goat $F(ab')_2$ Fragment anti-human IgG (Fcγ) Ab (Beckman Coulter). The cells were washed again and resuspended in cold PBS. The analysis was performed on an FACSCalibur flow cytometer with CellQuest software (BD Biosciences, Franklin Lakes, NJ). The mean specific fluorescence intensity (MSFI) was calculated as the ratio of the mean fluorescence intensity of NZ-1 to that of control mAb. Positive expression of podoplanin was defined as an MSFI of >2.0, and high-level expression of podoplanin was defined as an MSFI of >10.0.

Immunohistochemistry

Tissue arrays of human mesothelioma were obtained from Biomax (Rockville, MD). Staining was performed using R.T.U. VECTASTAIN Elite ABC Kit (Vector Laboratories, Burlingame, CA) (40). The tissue arrays were steamed in sodium citrate buffer for 10 min using a microwave to retrieve Ag and incubated in 3% H_2O_2 for 30 min to inhibit endogenous peroxidase. After incubation in blocking serum for 20 min, the slides were incubated overnight with NZ-1, NZ-8, or D2-40 at 4°C. The slides were washed and incubated in prediluted biotinylated secondary Ab for 30 min, followed by incubation in ready-to-use streptavidin/peroxidase complex reagent for 30 min. The tissue arrays were developed with a diaminobenzidine substrate kit (Vector Laboratories) and counterstained with Mayer's hematoxylin (Muto Pure Chemicals, Tokyo, Japan).

Western blotting

Cells were rinsed with ice-cold PBS and lysed in M-PER reagent (Pierce, Rockford, IL) containing phosphatase and protease inhibitor cocktails (Roche, Indianapolis, IN). The concentrations of protein were determined using a Bio-Rad Protein Assay Kit (Bio-Rad, Hercules, CA). Cell lysate (15 μg/lane) was separated by SDS-PAGE. Immunoblotting was conducted as previously described (41).

Preparation of effector cells

Rat splenocytes were harvested from Wistar rat spleens. Spleens were minced, homogenized in RPMI 1640, and centrifuged after passing through the cell strainer (BD Biosciences) (40). The cell pellet was suspended in RBC lysis buffer (Sigma-Aldrich, St. Louis, MO) on ice for 10 min. After depletion of RBCs, splenocytes were resuspended in CRPMI 1640 and used as effector cells. The method by which SCID mouse splenocytes were harvested was the same as that of rat splenocytes. Human PBMCs (MNC) were obtained from leukocytes in lymphocyte separation medium (Litton Bionetics, Kensington, MD) as previously described (42). Leukocytes were separated from peripheral blood of healthy donors using an RS-6600 rotor of a Kubota KR-400 centrifuge (Kubota, Tokyo, Japan). The human study was approved by the ethics committee of University of Tokushima, and written informed consent was obtained from all of the subjects.

ADCC

ADCC was evaluated using a [^{51}Cr]release assay as described previously (40, 43). Target cells were targeted with 0.1 μCi [^{51}Cr]sodium chromate at 37°C for 1 h. ^{51}Cr-labeled target cells were placed in 96-well plates in triplicate. Effector cells and NZ-1, NZ-1 $F(ab')_2$ fragment, NZ-8, or control IgG were added to the plates. After 6 h incubation, 100 μl supernatant was measured in a γ counter (PerkinElmer, Waltham, MA). Percent of cytotoxicity was calculated from the following formula: percent specific lysis = $(E - S)/(M - S) \times 100$, where E is the release in the test sample, S is the spontaneous release, and M is the maximum release.

Complement-dependent cytotoxicity

CDC was determined by [^{51}Cr]release assay (40). Target cells were incubated with 0.1 μCi [^{51}Cr]sodium chromate at 37°C for 1 h. After in-

cubation, the cells were washed with CRPMI 1640 three times. ^{51}Cr-labeled cells were added into 96-well plates and incubated with baby rabbit complement (Cedarlane Laboratories, Ontario, Canada) at a dilution of 1:4 and NZ-1 (1 μg/ml), NZ-8 (1 μg/ml), or control IgG (1 μg/ml) for 6 h. [^{51}Cr]Release of the supernatant from each well (100 μl) was measured using a γ counter. Percent of cytotoxicity was calculated as above.

Depletion or separation of rat NK cells

Depletion of NK cells from rat splenocytes was performed using the anti-asialo GM1 Ab as follows. Harvested rat splenocytes were treated with anti-asialo GM1 Ab (Wako, Osaka, Japan) at room temperature for 30 min. After treatment, splenocytes were incubated with baby rabbit complement at 37°C for 30 min, then washed with CRPMI 1640 three times, and the number of cells for use in experiments was counted. Rat NK cells were separated from Wistar rat splenocytes using a magnetic cell-sorting system. Splenocytes were incubated with FITC-conjugated anti-CD161a Ab (BD Biosciences) at 4°C for 30 min and then with anti-FITC mAb-coupled superparamagnetic microbeads (Miltenyi Biotec, Auburn, CA) at 4°C for 15 min. CD161a-positive or -negative selection was carried out using an autoMACS (Miltenyi Biotec) according to the manufacturer's instructions (44). Isolated CD161a$^+$ and CD161a$^-$ cells that yielded purity ≥90 and ≥99.9%, respectively, as determined by flow cytometry were used in experiments. To purify CD14$^+$ cells and CD56$^+$ cells from human MNC, AutoMACS and CD14 or CD56 microbeads (Miltenyi Biotec) were used. Human MNC were treated with CD14 or CD56 microbeads at 4°C for 15 min, and then cells were separated by autoMACS. The purities of CD14$^+$ and CD56$^+$ cells were ≥90%.

Animal experiments

SCID mice were injected s.c. into the right flank with ACC-MESO-4 (4.0×10^6 cells) or MSTO-211H/PDPN (1.0×10^6 cells). Tumor size is expressed as tumor area (mm^2): the longest diameter × the shortest diameter. The tumor-bearing mice were divided into several experimental groups before treatment with Abs was initiated. An i.p. injection of NZ-1 (100 μg), NZ-1

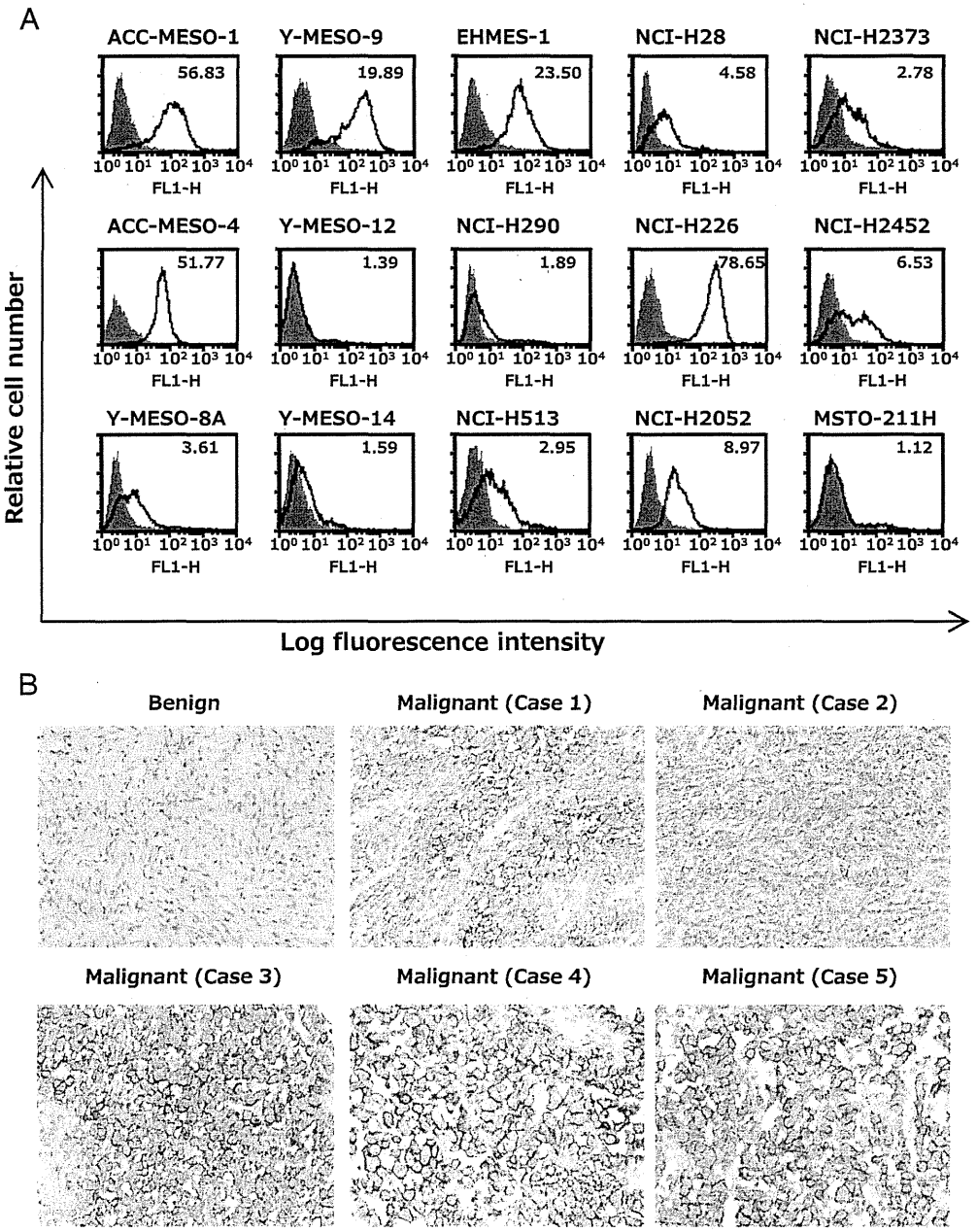

FIGURE 1. Expression of podoplanin in MM. (**A**) Expression of podoplanin in MPM cell lines was detected by flow cytometry. MPM cell lines were stained with NZ-1 (bold line) and control IgG (hatched area). The number in the top right corner in each figure is the MSFI. (**B**) Immunohistochemistry demonstrated the expression of podoplanin using the tissue array. Tissues were stained with 1 μg/ml of NZ-1 (original magnification ×200).

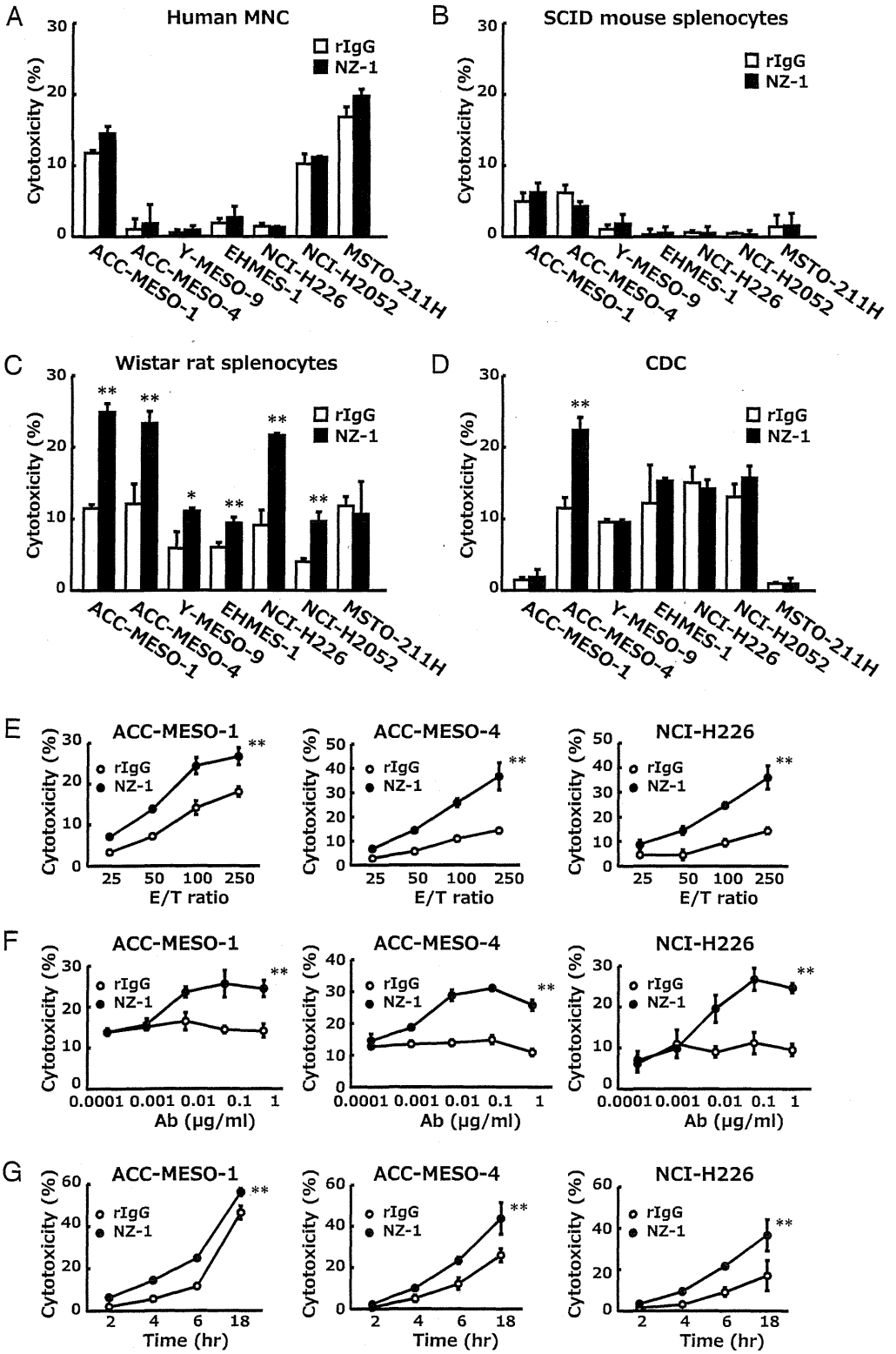

FIGURE 2. ADCC and CDC of NZ-1 against MPM cells. (**A–C**) ADCC activity of NZ-1 against various MPM cells was evaluated by 6-h [^{51}Cr]release assay in the presence of 1 μg/ml control rat IgG (rIgG; open column) or NZ-1 (filled column) at E:T ratio of 100. Human MNC (A), SCID mouse splenocytes (B), and Wistar rat splenocytes (C) were used as effector cells. (**D**) CDC activity of NZ-1 was determined using the 6-h [^{51}Cr]release assay in the presence of 1 μg/ml Ab with baby rabbit complement at a dilution of 1:4. E:T ratio (**E**) and dose dependence of NZ-1 (**F**) as well as time course of ADCC (**G**) were detected by [^{51}Cr]release assay using rat splenocytes as effector cells. Unchanged experimental conditions were 1 μg/ml Ab, 100 as the E:T ratio, and duration of 6 h. *$p < 0.05$ versus control, **$p < 0.01$ versus control (values are means ± SE).

$F(ab')_2$ fragment (67.5 μg), NZ-8 (100 μg), control rat IgG (100 μg), or control human IgG (100 μg) was started, on average, 14 d after tumor inoculation, when the tumor size had reached 15 (± 3 SD) mm^2, and continued twice a week for 2 wk. Rat $CD161a^+$ cells (1.0×10^5 cells), human $CD56^+$ cells (1.0×10^5 cells), or control normal saline injection (s.c.) around the tumors continued weekly for 2 wk.

In vivo fluorescence imaging

In vivo fluorescence imaging was performed using IVIS Spectrum (Caliper Life Sciences, Hopkinton, MA) (45). ACC-MESO-4 (4.0×10^6 cells) was injected into the right flank of SCID mice (s.c.). When the tumor grew to a sufficient size (25 mm^2), 100 μg NZ-1 or rat IgG labeled with XenoLight CF770 (Caliper Life Sciences) was injected (i.p.). The fluorescence in each mouse was determined using IVIS Spectrum (Caliper Life Sciences), with an excitation wavelength of 730–760 nm and an emission wavelength of 830–850 nm, every day after the labeled Ab injection. Mice were anesthetized with isoflurane (Abbott Laboratories, Chicago, IL). Images were acquired and analyzed using Living Image 3.1 software (Caliper Life Sciences).

Statistical analyses

The statistical significance of differences in in vitro and in vivo data were analyzed by Student *t* test and one-way ANOVA. In this study, *p* values <0.05 were considered significant in all experiments.

Results

Detection of podoplanin expression in MPM cell lines and tissues

First, we evaluated the expression of podoplanin on the surface of MPM cells using NZ-1, which is highly reactive for podoplanin. Fig. 1A shows that MPM cells expressed various levels of podoplanin as determined by flow cytometry. Expression of podoplanin was detected on 73% (11 out of 15) of MPM cells, and sarcomatoid type showed a higher expression rate of 100% (3 out of 3) as compared with 75% of epithelioid type (6 out of 8) and 50% of biphasic type (2 out of 4), although the number of cell lines is not sufficient to determine the expression rate. High level of expression of podoplanin, which is defined as a ratio of the mean fluorescence intensity of NZ-1 to that of control IgG of >10, was found in 33% (5 out of 15) of all cells, of which four cell lines are in an epithelioid type.

We next examined podoplanin expression in tissues of mesothelioma by immunohistochemistry with NZ-1. As shown in Fig. 1B, strong intensity of podoplanin staining was observed in tissues of MM, except benign mesothelioma. Podoplanin expression was found in 92% (33 out of 36) of all MM tissues.

ADCC and CDC mediated by NZ-1 against MPM cells

Next, we attempted to clarify whether NZ-1 has the potential to induce ADCC-targeted MPM cells expressing podoplanin. As shown in Fig. 2A and 2B, using human MNC or SCID mouse splenocytes as effector cells, we could not detect ADCC induced by NZ-1. By contrast, significant ADCC against only podoplanin-positive, but not podoplanin-negative, MPM cells was induced by NZ-1 when splenocytes of Wistar rat were used as effector cells (Fig. 2C). The level of ADCC was strongly associated with the level of podoplanin expression (Figs. 1A, 2C). In contrast, CDC induced by NZ-1 was detected only against ACC-MESO-4 cells (Fig. 2D). Additionally, treatment with 1 μg/ml NZ-1 alone did not inhibit proliferation of these MPM cell lines, indicating that NZ-1 has no direct growth-inhibitory activity on MPM cells in our experimental conditions (data not shown).

To evaluate the kinetics of ADCC activity mediated by NZ-1, we analyzed the E:T ratio and time course of ADCC and dose dependence of NZ-1. As shown in Fig. 2E, the level of ADCC was dependent on E:T ratio. In addition, NZ-1 also effectively induced ADCC against podoplanin-expressing cells in a dose- and time-dependent manner (Fig. 2F, 2G). The optimal concentration of NZ-1 to induce ADCC seems to be >0.1 μg/ml. These results suggest that rat anti-podoplanin Ab NZ-1 exhibits potent ADCC against MPM cells.

NZ-1 induces ADCC against podoplanin-transfected MPM cell lines

To confirm that ADCC of NZ-1 depends on the expression of podoplanin on target cells, we used MSTO-211H/PDPN as target

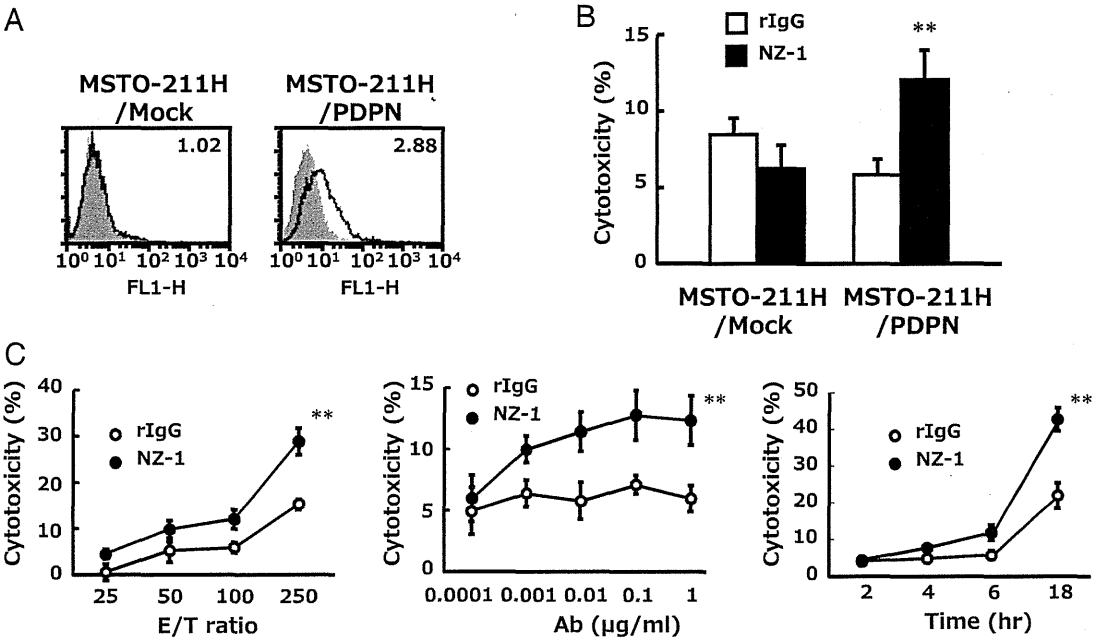

FIGURE 3. NZ-1 induces ADCC against MSTO-211H transfected with podoplanin. (**A**) Expression of podoplanin was detected by FACS analysis. (**B**) ADCC activity of NZ-1 using rat splenocytes against MSTO-211H/PDPN was evaluated by 6-h [^{51}Cr]release assay in the presence of 1 μg/ml Ab at the E:T ratio of 100. (**C**) E:T ratio–, dose-, and time-dependent effects of ADCC against MSTO-211H/PDPN mediated by NZ-1 with rat splenocytes were demonstrated by [^{51}Cr]release assay. $^{**}p < 0.01$ versus control (values are means ± SE). rIgG, rat IgG.

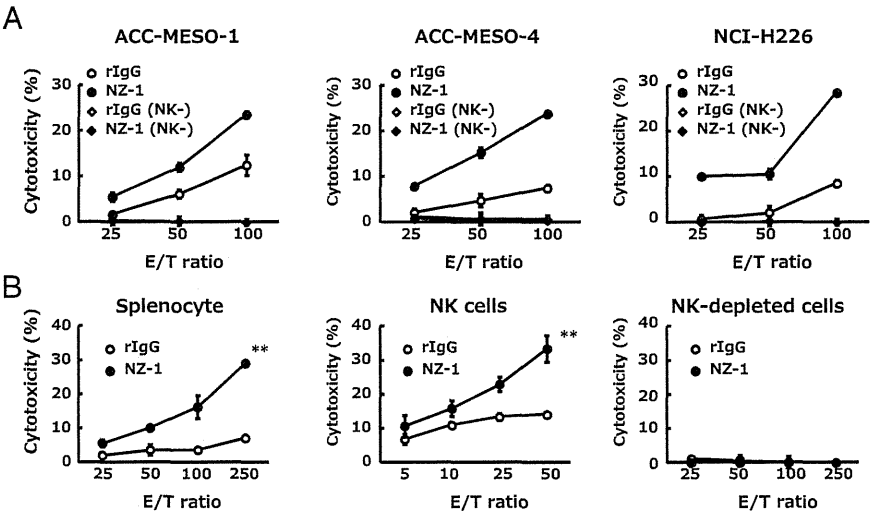

FIGURE 4. Rat NK cells are the main effector cells in ADCC induced by NZ-1. (**A**) Effects of depletion of NK cells from rat splenocytes on ADCC by NZ-1. NK cells in rat splenocytes were depleted by treatment of anti-asialo GM1 Ab and baby rabbit complement. (**B**) Rat NK cells are involved in ADCC activity of NZ-1. NK ($CD161a^+$) cells or NK-removed ($CD161a^-$) cells were isolated from rat splenocytes by AutoMACS. ADCC activity of 1 μg/ml Ab for 6 h was examined in ACC-MESO-4 as a target cell. $^{**}p < 0.01$ versus control (values are means ± SE). rIgG, Rat IgG.

cells. MSTO-211H/PDPN was generated by transfecting pcDNA3/podoplanin into MSTO-211H, one of the podoplanin-negative MPM cell lines (Fig. 3A). Although ADCC of NZ-1 was not detected against MSTO-211H/Mock, NZ-1 exhibited significant ADCC activity against MSTO-211H/PDPN (Fig. 3B). E:T ratio–, dose-, and time-dependent ADCC activities against MSTO-211H/PDPN were also induced by NZ-1 (Fig. 3C).

ADCC of NZ-1 is mediated by rat NK cells

For further investigation of the type of effector cells in rat splenocytes, we depleted NK cells using anti-asialo GM1 Ab and baby rabbit complement. As shown in Fig. 4A, ADCC was not induced by NK cell–depleted splenocytes. Moreover, we isolated NK ($CD161a^+$) cells and examined ADCC using NZ-1 against ACC-MESO-4. Fig. 4B shows that the purified NK ($CD161a^+$) cells from rat splenocytes showed a significant level of ADCC. In contrast, $CD161a^-$ splenocytes did not induce ADCC by NZ-1.

Antitumor activity of NZ-1 on the growth of podoplanin-expressing MPM cells in vivo

To evaluate the antitumor activity of NZ-1 in vivo, we used s.c. xenograft of human MPM (ACC-MESO-4) in SCID mice. NZ-1 or control rat IgG was injected i.p. twice a week, and rat NK ($CD161a^+$) cells or normal saline was injected s.c. weekly for 2 wk because ADCC of NZ-1 was mediated only by rat NK cells but not mouse splenocytes. Treatment with NZ-1 was started when tumors were established and formed a visible tumor mass (>15 mm^2) owing to the evaluation of therapeutic antitumor ability of NZ-1. The antitumor activity of NZ-1 against ACC-MESO-4 in vivo is shown in Fig. 5A. Administration of NZ-1 with rat NK ($CD161a^+$) cells significantly inhibited the growth of ACC-MESO-4 cells. By contrast, the injection of neither NZ-1 nor NK ($CD161a^+$) cells alone showed antitumor effects in our experimental setting. Using an MSTO-211H/PDPN xenograft model, tumor growth was also significantly inhibited by treatment with NZ-1 and NK ($CD161a^+$) cells (Fig. 5B).

Critical contribution of Fc portion to antitumor activity of NZ-1

It is known that ADCC activity is mediated by binding of the Fc portion of Abs to the FcR on NK cells. Therefore, we examined the antitumor activity of NZ-1 $F(ab')_2$ fragment. Although the NZ-1 F $(ab')_2$ fragment recognized podoplanin on ACC-MESO-4 in flow cytometric analysis to a similar extent as intact NZ-1, the $F(ab')_2$ fragment did not induce ADCC against ACC-MESO-4 (Fig. 6A,

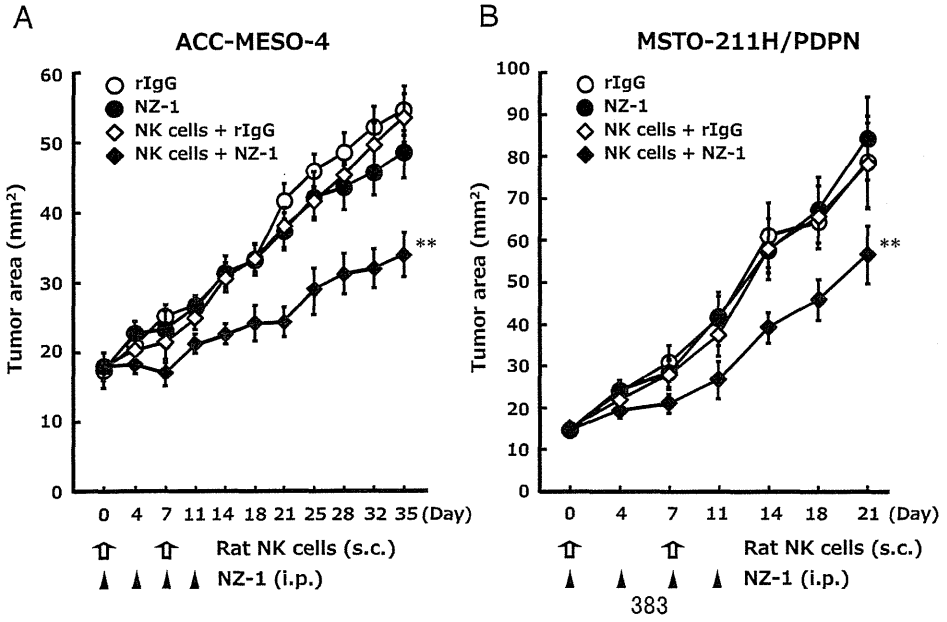

FIGURE 5. Antitumor activity of NZ-1 against MPM cells in vivo. SCID mice ($n = 5$) were injected s.c. with 4.0×10^6 ACC-MESO-4 cells (**A**) or 1.0×10^6 MSTO-211H/PDPN cells (**B**). NZ-1 (100 μg) or control rat IgG (rIgG; 100 μg) injection (i.p.) was continued twice a week for 2 wk. Rat NK ($CD161a^+$) cell (1.0×10^5 cells) injection (s.c.) around the tumors continued weekly for 2 wk. $^{**}p < 0.01$ versus control (values are means ± SE).

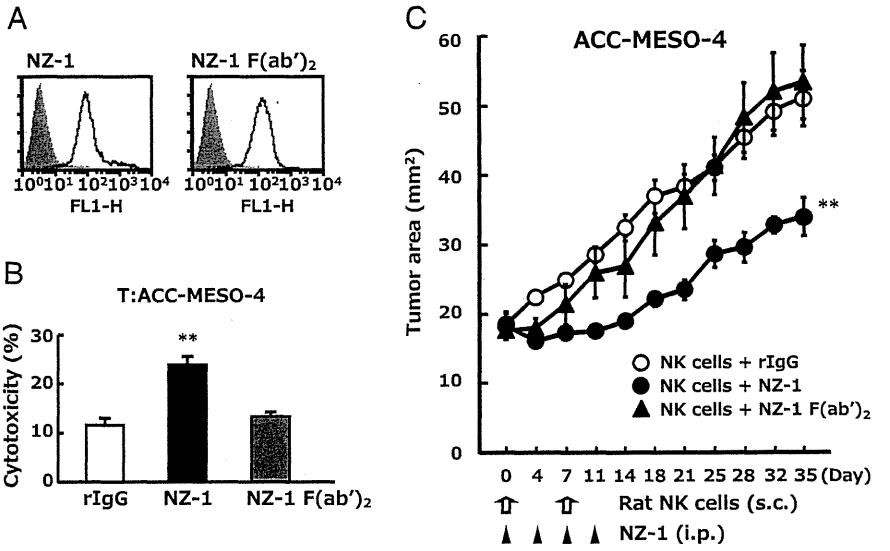

FIGURE 6. Critical contribution of Fc portion to antitumor activity of NZ-1. (**A**) Binding ability of NZ-1 F(ab')$_2$ fragment to podoplanin on the cell surface was compared with that of NZ-1 by FACS analysis. (**B**) ADCC activity against ACC-MESO-4 was evaluated by [^{51}Cr]release assay in the presence of control rat IgG (rIgG), NZ-1, or NZ-1 F(ab')$_2$ fragment with rat splenocytes. (**C**) Antitumor effect of NZ-1 (100 μg), NZ-1 F(ab')$_2$ fragment (67.5 μg), or control rIgG (100 μg) injection (i.p.) was evaluated using ACC-MESO-4 s.c. xenograft SCID mouse model ($n = 5$). $^{**}p < 0.01$ versus control (values are means ± SE).

6B). Moreover, i.p. injection of NZ-1 F(ab')$_2$ fragment unalterably showed no effect on tumor growth of ACC-MESO-4 compared with intact NZ-1, even when rat NK cells were simultaneously administered (Fig. 6C).

In vivo accumulation of injected NZ-1 to MPM xenograft in SCID mice

Next, we investigated the accumulation of injected NZ-1 on s.c. podoplanin-positive MPM tumor in SCID mouse model. As shown in Fig. 7A, Xenolight CF770-labeled NZ-1 accumulated on s.c. ACC-MESO-4 after single i.p. injection. Quantification of accumulation to the tumor of NZ-1 or control rat IgG showed a peak of the accumulation of NZ-1 on day 5, and the accumulation could be detected over 3 wk (Fig. 7B).

Immunostaining of podoplanin expressing in MPM and normal tissue with a novel rat-human chimeric anti-human podoplanin Ab NZ-8

Because it was demonstrated that NZ-1 showed antitumor activity through ADCC mediated by rat NK cells, to apply targeted therapy

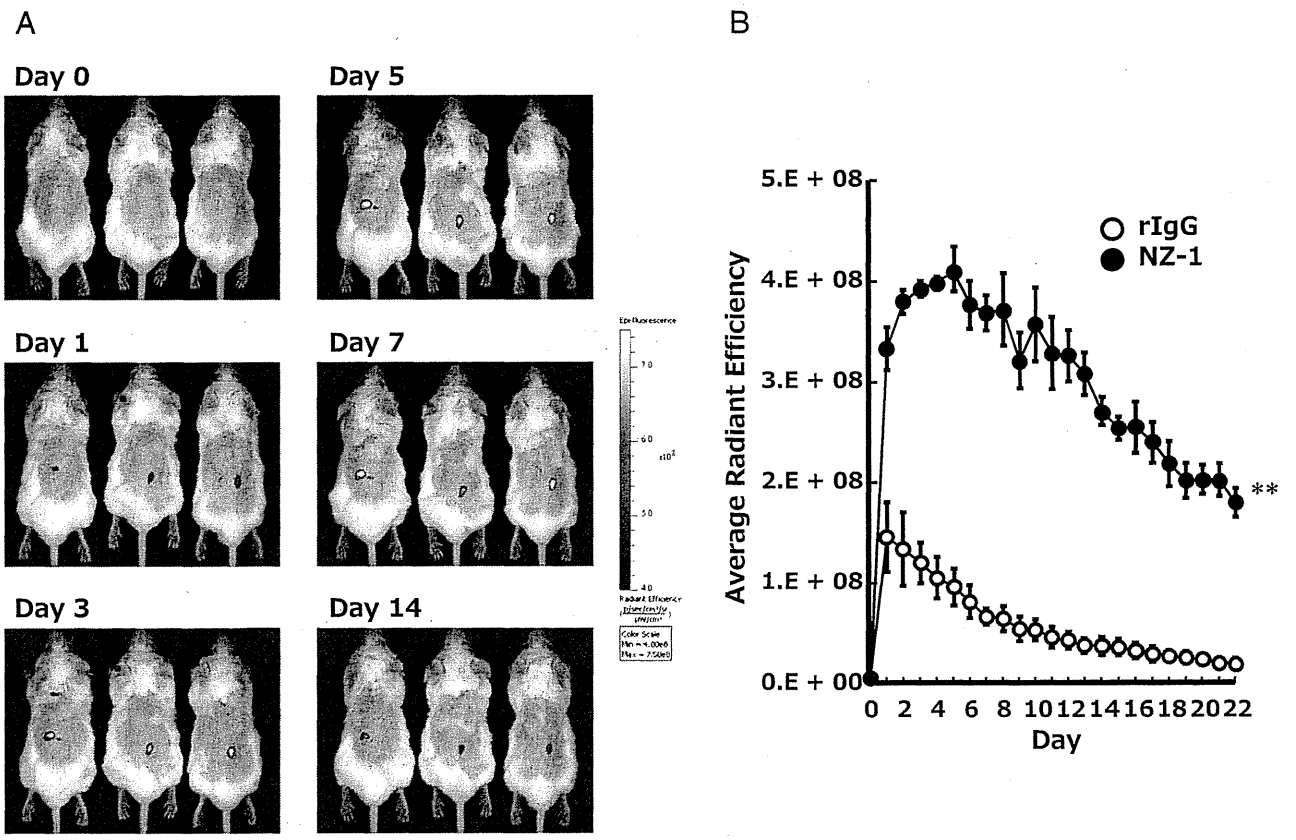

FIGURE 7. In vivo fluorescence imaging of NZ-1 in MPM xenograft model in SCID mice. (**A**) Fluorescence-labeled NZ-1 (100 μg) or control rat IgG (rIgG; 100 μg) was injected once i.p. to ACC-MESO-4 s.c. xenograft SCID mouse model ($n = 3$). (**B**) Accumulation of fluorescence in s.c. tumors was calculated and analyzed using IVIS Spectrum (Caliper Life Sciences) every day after the labeling Ab injection. $^{**}p < 0.01$ versus control (values are means ± SE).

to podoplanin with Ab in a clinic, we generated the chimeric Ab by fusing the V_H and V_L regions of rat Ab (NZ-1) with the C_H and C_L regions of human IgG_1, respectively (Fig. 8A). As shown in Fig. 8B and 8C, NZ-8, a novel rat-human chimeric anti-human podoplanin Ab, could recognize the podoplanin expressing in MPM like NZ-1 by flow cytometry as well as immunohistochemistry. Moreover, to confirm the recognition pattern of NZ-8 to podoplanin, the lysate of MPM cells were subjected to Western blotting. As shown in Fig. 8D, NZ-8 could detect the ladder bands of podoplanin. However, the recognizing pattern of NZ-8 was different from that of D2-40. Thinking of clinical application of NZ-8, the recognition of podoplanin expressing in normal tissue by NZ-8 is quite important. Therefore, we examined the staining pattern of podoplanin expressing in normal tissue such as lymphatic vessels, alveolar epithelial cells, and podocytes in the kidney by immunohistochemistry with NZ-8 because these tissues have been reported to express podoplanin. As shown in Fig. 8E, NZ-8 preferentially recognized the podoplanin expressing in MPM, but not in normal tissues including lymphatic vessels, alveolar epithelial cells, and podocytes. However, D2-40 strongly detected the podoplanin expressing in lymphatic vessels as compared with MPM tissues.

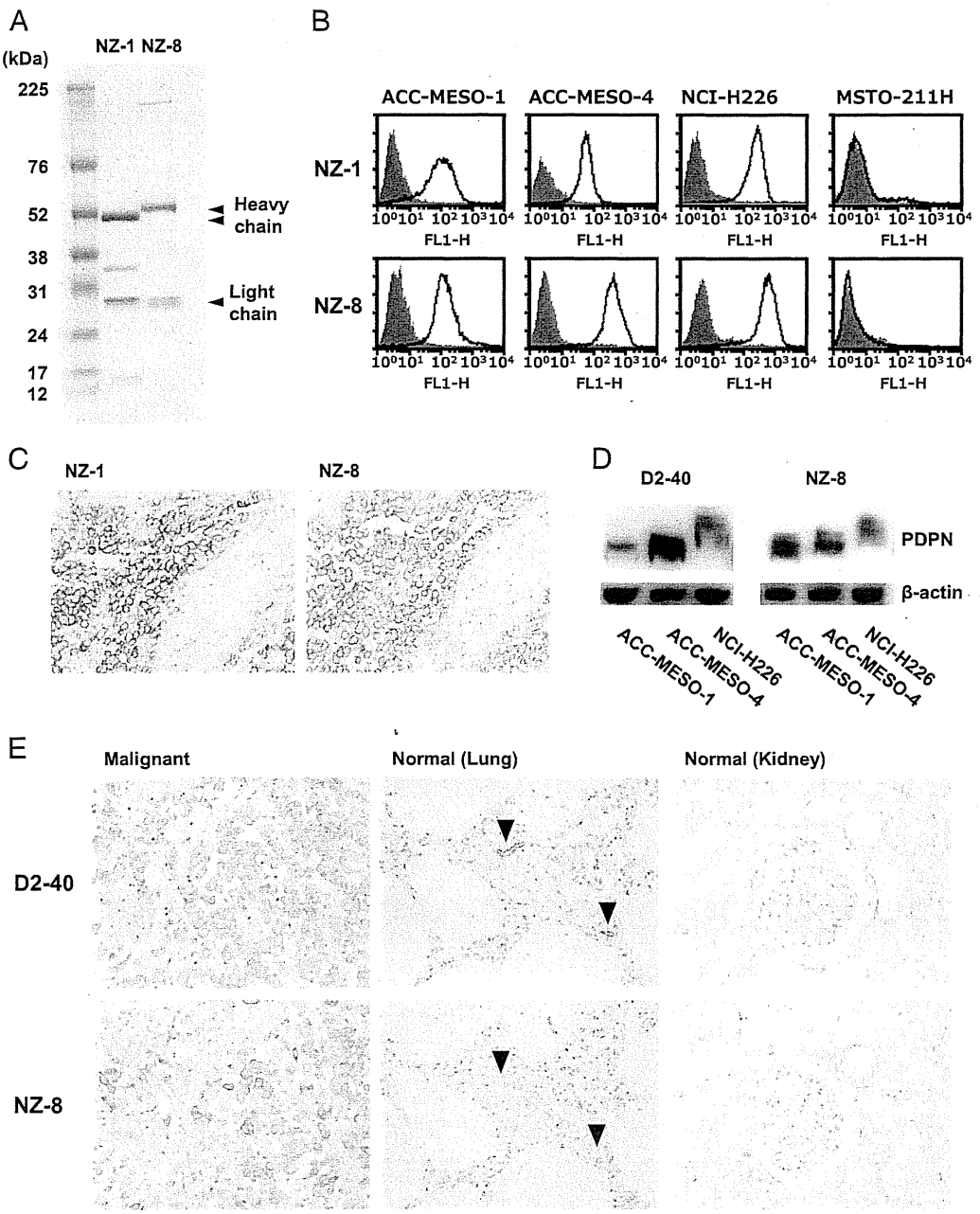

FIGURE 8. Immunostaining of podoplanin expressing in MPM and normal tissue with NZ-8. (**A**) SDS-PAGE of NZ-1 and NZ-8. SDS-PAGE using 5–20% gel was performed for purified NZ-1 and NZ-8 under the reducing condition. (**B**) Expression of podoplanin in MPM cell lines was detected by flow cytometry. MPM cell lines were stained with NZ-1 or NZ-8 (bold line) and control IgG (hatched area). (**C**) Immunohistochemistry demonstrated the detection of podoplanin expression using the tissue array. Tissues were stained with NZ-1 (1 μg/ml) or NZ-8 (1 μg/ml) (original magnification ×200). (**D**) Podoplanin (PDPN) protein in MPM cell lines was recognized by Western blotting proved with D2-40 (1:500) or NZ-8 (0.1 μg/ml). (**E**) The expression of podoplanin was examined in lymphatic vessels (arrowheads) and type I alveolar epithelium (lung) and podocyte (kidney) as well as MM using the tissue array. The slides of the tissue array were stained with D2-40 (1:500) or NZ-8 (0.1 μg/ml) (original magnification ×200).

In vitro and in vivo antitumor activity of NZ-8 against MPM cells

We further assessed whether NZ-8 can induce antitumor effect against MPM cells mediated by human MNC as effector cells. As shown in Fig. 9A, ADCC against MPM cell lines was not exhibited by NZ-1 with human MNC, whereas NZ-8 showed the induction of a significant level of ADCC mediated by human MNCs against podoplanin-positive MPM cells but not podoplanin-negative MPM cells. CDC was also induced by NZ-8 against ACC-MESO-4 and NCI-H226, which was significantly higher than that of NZ-1 (Fig. 9B). Further effector cell analysis of ADCC clearly demonstrated that human NK ($CD56^+$) cells, but not human monocytes ($CD14^+$); could induce ADCC by NZ-8 (Fig. 9C). Using the xenograft model of ACC-MESO-4 in SCID mice, the tumor growth was also significantly inhibited by treatment with NZ-8 and human NK ($CD56^+$) cells (Fig. 9D). By contrast, no antitumor effects were shown by the injection of NZ-8 or human NK ($CD56^+$) cells alone. Furthermore, administration of NZ-1 did not show any antitumor effects when human NK ($CD56^+$) cells were used as an effector cells (Fig. 9E).

Discussion

In the current study, we have demonstrated that a rat anti-human podoplanin mAb, NZ-1, possesses potent ADCC mediated by rat NK cells and CDC activity and mediates in vivo therapeutic antitumor activity against MPM in SCID mice. Moreover, we have also shown that a novel rat-human chimeric anti-human podoplanin Ab, NZ-8, effectively induces ADCC mediated by human NK cells and CDC and mediates in vivo antitumor activity against MPM cells. Furthermore, NZ-8 preferentially recognized the podoplanin expressing in MPM than those in normal tissues. These results strongly suggest the possible clinical application of anti-human podoplanin Ab against MPM.

In this study, we found that podoplanin was expressed on 73% of MPM cell lines including 33% of high-expression and 92% of MM tissues, which is consistent with previous studies (46–48). Furthermore, NZ-8 could recognize the expression of podoplanin in MPM like NZ-1. Compared with other mesothelioma-associated Ags such as calretinin, thrombomodulin, cytokeratin 5, WT1, and mesothelin in previous studies (47–49), the frequency of expression of podoplanin is the same or higher than that of others, suggesting that podoplanin could be a novel immunological target for MPM therapy. In contrast, although it was reported that podoplanin was expressed in lymphatic vessels and type I alveolar epithelium and podocyte (15–17), NZ-8 could not detect the expression of podoplanin in lymphatic vessels when it was used at the lower concentration of 0.1 μg/ml, which could still recognize the podoplanin in MPM tissues and induce the ADCC and CDC reactions. This staining pattern of NZ-8 is quite different from that

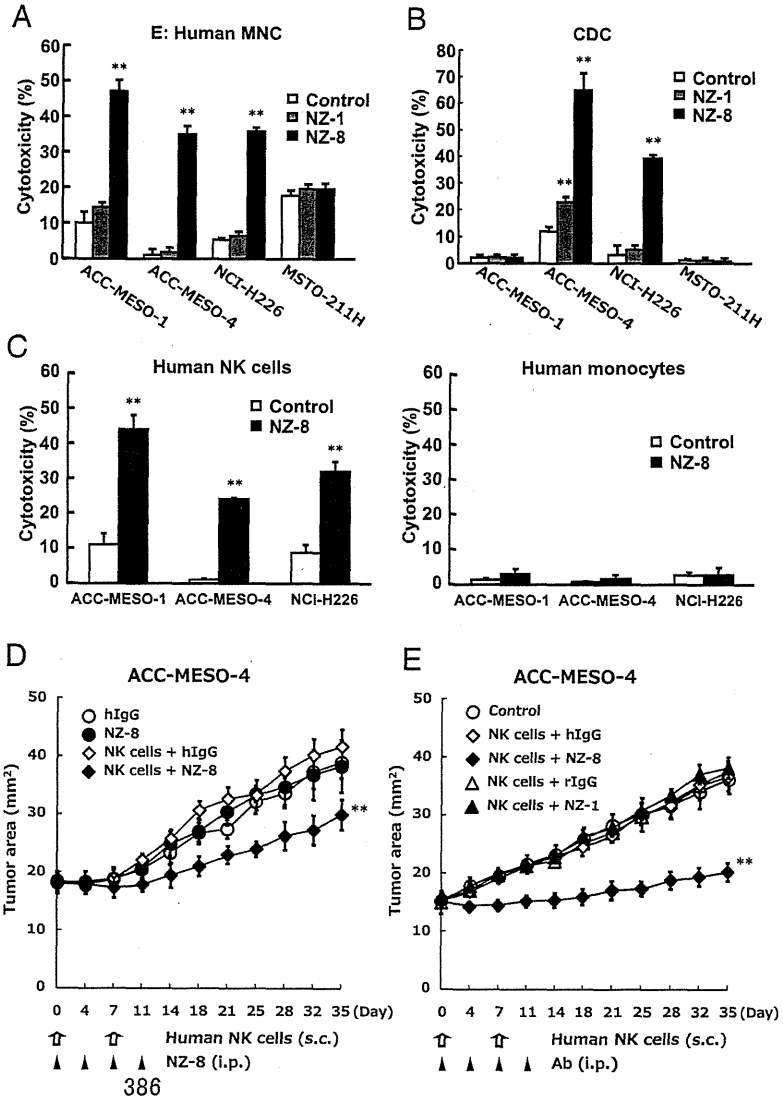

FIGURE 9. Antitumor activity of NZ-8 in vitro and in vivo. (**A**) ADCC induced by human MNC against MPM cell lines, ACC-MESO-1, ACC-MESO-4, NCI-H226, and MSTO-211H, was determined with 6-h [^{51}Cr]release assay at the E:T ratio of 100 in the presence of 1 μg/ml NZ-1 or NZ-8. (**B**) CDC activity was demonstrated by [^{51}Cr]release assay. The experimental condition was the same as for Fig. 2D. (**C**) Human NK cells are the main effector cells in ADCC activity of NZ-8. NK ($CD56^+$) cells or monocytes ($CD14^+$) were isolated from human MNC by AutoMACS. ADCC activity of 1 μg/ml NZ-8 mediated by NK ($CD56^+$) cells or monocytes ($CD14^+$) was evaluated by 6-h [^{51}Cr]release assay at E:T ratio of 10 or 50. SCID mice ($n = 5$) were injected s.c. with 4.0×10^6 ACC-MESO-4 cells. NZ-8 (100 μg) or human IgG (hIgG; 100 μg) (**D**), and NZ-1 (100 μg), NZ-8 (100 μg), or rat IgG (rIgG; 100 μg), and human IgG (hIgG; 100 μg) (**E**) injection (i.p.) was continued twice a week for 2 wk. Human NK ($CD56^+$) cell (1.0×10^5 cells) injection (s.c.) around the tumors continued weekly for 2 wk. $^{**}p < 0.01$ versus control (values are means ± SE).

of D2-40, which has been frequently used as an anti-podoplanin Ab in many studies (46, 47, 50). The reason why NZ-8 preferentially recognizes the podoplanin expressing in MPM, but not in normal tissues, is still unclear. However, it might be due to the difference in the epitopes recognized by each Ab in addition to the difference in the expression level of podoplanin between MPM and normal tissues, because we have shown that the epitope recognized by NZ-1 is platelet aggregation-stimulating domain-2/3, and the epitope of D2-40 is platelet aggregation-stimulating 1/2 (32). In the current study, it is considered that the recognition pattern of NZ-8, which possesses V_H and V_L of NZ-1, was also different from that of D2-40.

Originally, NZ-1 showed high binding affinity against podoplanin ($K_D = 1.2 \times 10^{-10}$ M) (33). In addition, it has been demonstrated that NZ-1 suppresses podoplanin-induced pulmonary metastasis through inhibiting platelet aggregation (27). In the current study, NZ-1 showed other effector functions, for ADCC and CDC. Recently, therapeutic Abs have been classified into three classes (34), in which class I Abs are defined to possess ADCC and CDC and ranked in the highly potential category, especially for cancer immunotherapy. On the basis of this concept, NZ-1 seems to be ranked as a highly potent therapeutic Ab because it has effector functions such as ADCC and CDC in addition to preventing metastasis by inhibiting platelet aggregation.

ADCC activity of NZ-1 has not been reported because NZ-1 did not show any ADCC activity mediated by murine splenocytes or human MNCs. However, when ADCC of NZ-1 was examined using rat splenocytes, significant ADCC activity was detected. To use rat splenocytes as effector cells is unusual to evaluate the ADCC activity of Ab; however, other studies have also reported that, in special cases, rat splenocytes are more useful than murine ones for testing the ADCC activity of rat mAb (51, 52). If the Ab has potency to induce the ADCC mediated by effector cells of several species except for humans effectively, it would be possible to prepare chimeric or humanized Ab that induces ADCC mediated by human effector cells. Therefore, from our study, it is also noted that rat splenocytes have the same importance to screen the ADCC activity of Ab as human MNC or mouse splenocytes.

In vivo experiments have shown that NZ-1 reduces the tumor growth of s.c. inoculated cell lines of both ACC-MESO-4 and MSTO-211H/PDPN, suggesting that NZ-1 possesses antitumor effects against MPM as well. In addition, it is very important that antitumor effects of NZ-1 were observed against established tumors, indicating that treatment with NZ-1 was apparently therapeutic, not preventive. Previously, we reported that NZ-1 directly inhibits podoplanin-dependent tumor metastasis in vivo (27). By contrast, in this study, administration of NZ-1 alone had no effect to reduce the podoplanin-positive MPM cell growth in SCID mice. The suppressive effects on tumor growth of NZ-1 are required for the administration with rat NK cells, probably as immune effector cells. In addition, NZ-1 $F(ab')_2$ fragment induced neither ADCC in vitro nor antitumor effect in vivo, which supports the notion that interaction between Fc portion of the Ab and FcR of the effector cell leads to the antitumor effect of NZ-1. Moreover, in vivo fluorescence imaging results have demonstrated that injected NZ-1 specifically accumulates to s.c. ACC-MESO-4. Recent study has shown that tumor accumulation of trastuzumab, which is an anti-Her2 Ab widely used against Her2-positive breast cancer in a clinical context, peaked at 24 h and decreased at the same rate as the baseline after 24 h in SCID mice model (53). By contrast, in this study, specific accumulation of NZ-1 peaked at day 5 and could continue over 3 wk after a single injection. Recently, we have also shown that NZ-1 was selectively accumulated to podoplanin-positive glioblastoma but not normal tissues (33). Therefore, it was estimated that NZ-1 has strong binding affinity and specific accumulation potential against target Ags. These results indicated that NZ-1 might have strong antitumor effects against MPM in vivo by ADCC.

Finally, we have shown that NZ-8, a novel rat-human chimeric anti-human podoplanin Ab, generated from NZ-1 has the potency to induce ADCC against MPM cells mediated by human NK cells as effector cells. Interestingly, the level of ADCC and CDC of NZ-8 was significantly higher than that of NZ-1. Moreover, NZ-8 has the promising antitumor effects against MPM cells mediated by human NK cells in vivo, in contrast to administration of NZ-1 with human NK cells, which did not induce any antitumor effects. In addition, NZ-8 preferentially detected the podoplanin expressing in MPM, but not in normal tissues.

In conclusion, we found that both NZ-1 and NZ-8 possess potent and therapeutic antitumor effects based on ADCC against MPM in an SCID mouse model. Importantly, NZ-8 could induce higher ADCC mediated by human NK cells in addition to CDC as compared with NZ-1. Based on the ability of NZ-8, which preferentially recognizes the podoplanin expressing in MPM, but not in normal tissues, the current study suggests that targeting therapy to podoplanin using NZ-8 might be useful for patients with MPM as a novel immunotherapy.

Acknowledgments

We thank Tomoko Oka, Imi Saito, Ryo Yanagiya, Shunpei Morita, Kana Nasu, Hiroko Sasaki, Sachiko Suzuki, and Junko Aita for excellent technical assistance.

Disclosures

The authors have no financial conflicts of interest.

References

1. Robinson, B. W., and R. A. Lake. 2005. Advances in malignant mesothelioma. *N. Engl. J. Med.* 353: 1591–1603.
2. Pelucchi, C., M. Malvezzi, C. La Vecchia, F. Levi, A. Decarli, and E. Negri. 2004. The Mesothelioma epidemic in Western Europe: an update. *Br. J. Cancer* 90: 1022–1024.
3. Murayama, T., K. Takahashi, Y. Natori, and N. Kurumatani. 2006. Estimation of future mortality from pleural malignant mesothelioma in Japan based on an age-cohort model. *Am. J. Ind. Med.* 49: 1–7.
4. Ray, M., and H. L. Kindler. 2009. Malignant pleural mesothelioma: an update on biomarkers and treatment. *Chest* 136: 888–896.
5. Vogelzang, N. J., J. J. Rusthoven, J. Symanowski, C. Denham, E. Kaukel, P. Ruffie, U. Gatzemeier, M. Boyer, S. Emri, C. Manegold, et al. 2003. Phase III study of pemetrexed in combination with cisplatin versus cisplatin alone in patients with malignant pleural mesothelioma. *J. Clin. Oncol.* 21: 2636–2644.
6. Scherpereel, A., P. Astoul, P. Baas, T. Berghmans, H. Clayson, P. de Vuyst, H. Dienemann, F. Galateau-Salle, C. Hennequin, G. Hillerdal, et al; European Respiratory Society/European Society of Thoracic Surgeons Task Force. 2010. Guidelines of the European Respiratory Society and the European Society of Thoracic Surgeons for the management of malignant pleural mesothelioma. *Eur. Respir. J.* 35: 479–495.
7. Inamoto, T., T. Yamada, K. Ohnuma, S. Kina, N. Takahashi, T. Yamochi, S. Inamoto, Y. Katsuoka, O. Hosono, H. Tanaka, et al. 2007. Humanized anti-CD26 monoclonal antibody as a treatment for malignant mesothelioma tumors. *Clin. Cancer Res.* 13: 4191–4200.
8. Inami, K., M. Abe, K. Takeda, Y. Hagiwara, M. Maeda, T. Segawa, M. Suyama, S. Watanabe, and O. Hino. 2010. Antitumor activity of anti-C-ERC/mesothelin monoclonal antibody in vivo. *Cancer Sci.* 101: 969–974.
9. Krug, L. M., T. Dao, A. B. Brown, P. Maslak, W. Travis, S. Bekele, T. Korontsvit, V. Zakhaleva, J. Wolchok, J. Yuan, et al. 2010. WT1 peptide vaccinations induce CD4 and CD8 T cell immune responses in patients with mesothelioma and non-small cell lung cancer. *Cancer Immunol. Immunother.* 59: 1467–1479.
10. Hassan, R., S. J. Cohen, M. Phillips, I. Pastan, E. Sharon, R. J. Kelly, C. Schweizer, S. Weil, and D. Laheru. 2010. Phase I clinical trial of the chimeric anti-mesothelin monoclonal antibody MORAb-009 in patients with mesothelin-expressing cancers. *Clin. Cancer Res.* 16: 6132–6138.
11. Kato, Y., N. Fujita, A. Kunita, S. Sato, M. Kaneko, M. Osawa, and T. Tsuruo. 2003. Molecular identification of Aggrus/T1alpha as a platelet aggregation-inducing factor expressed in colorectal tumors. *J. Biol. Chem.* 278: 51599–51605.
12. Kaneko, M. K., Y. Kato, T. Kitano, and M. Osawa. 2006. Conservation of a platelet activating domain of Aggrus/podoplanin as a platelet aggregation-inducing factor. *Gene* 378: 52–57.

13. Kaneko, M., Y. Kato, A. Kunita, N. Fujita, T. Tsuruo, and M. Osawa. 2004. Functional sialylated O-glycan to platelet aggregation on Aggrus (T1alpha/Podoplanin) molecules expressed in Chinese hamster ovary cells. *J. Biol. Chem.* 279: 38838–38843.
14. Hatakeyama, K., M. K. Kaneko, Y. Kato, T. Ishikawa, K. Nishihira, Y. Tsujimoto, Y. Shibata, Y. Ozaki, and Y. Asada. 2012. Podoplanin expression in advanced atherosclerotic lesions of human aortas. *Thromb. Res.* 129: e70–e76.
15. Breiteneder-Geleff, S., K. Matsui, A. Soleiman, P. Meraner, H. Poczewski, R. Kalt, G. Schaffner, and D. Kerjaschki. 1997. Podoplanin, novel 43-kd membrane protein of glomerular epithelial cells, is down-regulated in puromycin nephrosis. *Am. J. Pathol.* 151: 1141–1152.
16. Breiteneder-Geleff, S., A. Soleiman, H. Kowalski, R. Horvat, G. Amann, E. Kriehuber, K. Diem, W. Weninger, E. Tschachler, K. Alitalo, and D. Kerjaschki. 1999. Angiosarcomas express mixed endothelial phenotypes of blood and lymphatic capillaries: podoplanin as a specific marker for lymphatic endothelium. *Am. J. Pathol.* 154: 385–394.
17. Vanderbilt, J. N., L. Allen, R. F. Gonzalez, Z. Tigue, J. Edmondson, D. Ansaldi, A. M. Gillespie, and L. G. Dobbs. 2008. Directed expression of transgenes to alveolar type I cells in the mouse. *Am. J. Respir. Cell Mol. Biol.* 39: 253–262.
18. Kimura, N., and I. Kimura. 2005. Podoplanin as a marker for mesothelioma. *Pathol. Int.* 55: 83–86.
19. Kato, Y., M. Kaneko, M. Sata, N. Fujita, T. Tsuruo, and M. Osawa. 2005. Enhanced expression of Aggrus (T1alpha/podoplanin), a platelet-aggregation-inducing factor in lung squamous cell carcinoma. *Tumour Biol.* 26: 195–200.
20. Kato, Y., I. Sasagawa, M. Kaneko, M. Osawa, N. Fujita, and T. Tsuruo. 2004. Aggrus: a diagnostic marker that distinguishes seminoma from embryonal carcinoma in testicular germ cell tumors. *Oncogene* 23: 8552–8556.
21. Suzuki, H., Y. Kato, M. K. Kaneko, Y. Okita, H. Narimatsu, and M. Kato. 2008. Induction of podoplanin by transforming growth factor-beta in human fibrosarcoma. *FEBS Lett.* 582: 341–345.
22. Mishima, K., Y. Kato, M. K. Kaneko, R. Nishikawa, T. Hirose, and M. Matsutani. 2006. Increased expression of podoplanin in malignant astrocytic tumors as a novel molecular marker of malignant progression. *Acta Neuropathol.* 111: 483–488.
23. Wicki, A., F. Lehembre, N. Wick, B. Hantusch, D. Kerjaschki, and G. Christofori. 2006. Tumor invasion in the absence of epithelial-mesenchymal transition: podoplanin-mediated remodeling of the actin cytoskeleton. *Cancer Cell* 9: 261–272.
24. Martín-Villar, E., B. Fernández-Muñoz, M. Parsons, M. M. Yurrita, D. Megías, E. Pérez-Gómez, G. E. Jones, and M. Quintanilla. 2010. Podoplanin associates with CD44 to promote directional cell migration. *Mol. Biol. Cell* 21: 4387–4399.
25. Martín-Villar, E., D. Megías, S. Castel, M. M. Yurrita, S. Vilaró, and M. Quintanilla. 2006. Podoplanin binds ERM proteins to activate RhoA and promote epithelial-mesenchymal transition. *J. Cell Sci.* 119: 4541–4553.
26. Kunita, A., T. G. Kashima, Y. Morishita, M. Fukayama, Y. Kato, T. Tsuruo, and N. Fujita. 2007. The platelet aggregation-inducing factor aggrus/podoplanin promotes pulmonary metastasis. *Am. J. Pathol.* 170: 1337–1347.
27. Kato, Y., M. K. Kaneko, A. Kunita, H. Ito, A. Kameyama, S. Ogasawara, N. Matsuura, Y. Hasegawa, K. Suzuki-Inoue, O. Inoue, et al. 2008. Molecular analysis of the pathophysiological binding of the platelet aggregation-inducing factor podoplanin to the C-type lectin-like receptor CLEC-2. *Cancer Sci.* 99: 54–61.
28. Tsuneki, M., S. Maruyama, M. Yamazaki, J. Cheng, and T. Saku. 2012. Podoplanin expression profiles characteristic of odontogenic tumor-specific tissue architectures. *Pathol. Res. Pract.* 208: 140–146.
29. Yuan, P., S. Temam, A. El-Naggar, X. Zhou, D. D. Liu, J. J. Lee, and L. Mao. 2006. Overexpression of podoplanin in oral cancer and its association with poor clinical outcome. *Cancer* 107: 563–569.
30. Hoshino, A., G. Ishii, T. Ito, K. Aoyagi, Y. Ohtaki, K. Nagai, H. Sasaki, and A. Ochiai. 2011. Podoplanin-positive fibroblasts enhance lung adenocarcinoma tumor formation: podoplanin in fibroblast functions for tumor progression. *Cancer Res.* 71: 4769–4779.
31. Kato, Y., M. K. Kaneko, A. Kuno, N. Uchiyama, K. Amano, Y. Chiba, Y. Hasegawa, J. Hirabayashi, H. Narimatsu, K. Mishima, and M. Osawa. 2006. Inhibition of tumor cell-induced platelet aggregation using a novel anti-podoplanin antibody reacting with its platelet-aggregation-stimulating domain. *Biochem. Biophys. Res. Commun.* 349: 1301–1307.
32. Ogasawara, S., M. K. Kaneko, J. E. Price, and Y. Kato. 2008. Characterization of anti-podoplanin monoclonal antibodies: critical epitopes for neutralizing the interaction between podoplanin and CLEC-2. *Hybridoma (Larchmt)* 27: 259–267.
33. Kato, Y., G. Vaidyanathan, M. K. Kaneko, K. Mishima, N. Srivastava, V. Chandramohan, C. Pegram, S. T. Keir, C. T. Kuan, D. D. Bigner, and M. R. Zalutsky. 2010. Evaluation of anti-podoplanin rat monoclonal antibody NZ-1 for targeting malignant gliomas. *Nucl. Med. Biol.* 37: 785–794.
34. Jiang, X. R., A. Song, S. Bergelson, T. Arroll, B. Parekh, K. May, S. Chung, R. Strouse, A. Mire-Sluis, and M. Schenerman. 2011. Advances in the assessment and control of the effector functions of therapeutic antibodies. *Nat. Rev. Drug Discov.* 10: 101–111.
35. Kawaguchi, K., H. Murakami, T. Taniguchi, M. Fujii, S. Kawata, T. Fukui, Y. Kondo, H. Osada, N. Usami, K. Yokoi, et al. 2009. Combined inhibition of MET and EGFR suppresses proliferation of malignant mesothelioma cells. *Carcinogenesis* 30: 1097–1105.
36. Yokoyama, A., N. Kohno, S. Fujino, H. Hamada, Y. Inoue, S. Fujioka, and K. Hiwada. 1994. Origin of heterogeneity of interleukin-6 (IL-6) levels in malignant pleural effusions. *Oncol. Rep.* 1: 507–511.
37. Taniguchi, T., S. Karnan, T. Fukui, T. Yokoyama, H. Tagawa, K. Yokoi, Y. Ueda, T. Mitsudomi, Y. Horio, T. Hida, et al. 2007. Genomic profiling of malignant pleural mesothelioma with array-based comparative genomic hybridization shows frequent non-random chromosomal alteration regions including JUN amplification on 1p32. *Cancer Sci.* 98: 438–446.
38. Giovannetti, E., P. A. Zucali, Y. G. Assaraf, L. G. Leon, K. Smid, C. Alecci, F. Giancola, A. Destro, L. Gianoncelli, E. Lorenzi, et al. 2011. Preclinical emergence of vandetanib as a potent antitumour agent in mesothelioma: molecular mechanisms underlying its synergistic interaction with pemetrexed and carboplatin. *Br. J. Cancer* 105: 1542–1553.
39. Li, Q., W. Wang, T. Yamada, K. Matsumoto, K. Sakai, Y. Bando, H. Uehara, Y. Nishioka, S. Sone, S. Iwakiri, et al. 2011. Pleural mesothelioma instigates tumor-associated fibroblasts to promote progression via a malignant cytokine network. *Am. J. Pathol.* 179: 1483–1493.
40. Wang, W., Y. Nishioka, S. Ozaki, A. Jalili, S. Abe, S. Kakiuchi, M. Kishuku, K. Minakuchi, T. Matsumoto, and S. Sone. 2009. HM1.24 (CD317) is a novel target against lung cancer for immunotherapy using anti-HM1.24 antibody. *Cancer Immunol. Immunother.* 58: 967–976.
41. Kuramoto, T., H. Goto, A. Mitsuhashi, S. Tabata, H. Ogawa, H. Uehara, A. Saijo, S. Kakiuchi, Y. Maekawa, K. Yasutomo, et al. 2012. Dll4-Fc, an inhibitor of Dll4-notch signaling, suppresses liver metastasis of small cell lung cancer cells through the downregulation of the NF-κB activity. *Mol. Cancer Ther.* 11: 2578–2587.
42. Kishuku, M., Y. Nishioka, S. Abe, J. Kishi, H. Ogino, Y. Aono, M. Azuma, K. Kinoshita, R. Batmunkh, H. Makino, et al. 2009. Expression of soluble vascular endothelial growth factor receptor-1 in human monocyte-derived mature dendritic cells contributes to their antiangiogenic property. [Published erratum appears in 2010. *J. Immunol.* 185: 2630.] *J. Immunol.* 183: 8176–8185.
43. Wang, W., Y. Nishioka, S. Ozaki, A. Jalili, V. K. Verma, M. Hanibuchi, S. Abe, K. Minakuchi, T. Matsumoto, and S. Sone. 2009. Chimeric and humanized anti-HM1.24 antibodies mediate antibody-dependent cellular cytotoxicity against lung cancer cells. *Lung Cancer* 63: 23–31.
44. Nishioka, Y., N. Nishimura, Y. Suzuki, and S. Sone. 2001. Human monocyte-derived and CD83(+) blood dendritic cells enhance NK cell-mediated cytotoxicity. *Eur. J. Immunol.* 31: 2633–2641.
45. Zou, P., S. Xu, S. P. Povoski, A. Wang, M. A. Johnson, E. W. Martin, Jr., V. Subramaniam, R. Xu, and D. Sun. 2009. Near-infrared fluorescence labeled anti-TAG-72 monoclonal antibodies for tumor imaging in colorectal cancer xenograft mice. *Mol. Pharm.* 6: 428–440.
46. Chu, A. Y., L. A. Litzky, T. L. Pasha, G. Acs, and P. J. Zhang. 2005. Utility of D2-40, a novel mesothelial marker, in the diagnosis of malignant mesothelioma. *Mod. Pathol.* 18: 105–110.
47. Ordóñez, N. G. 2006. The diagnostic utility of immunohistochemistry and electron microscopy in distinguishing between peritoneal mesotheliomas and serous carcinomas: a comparative study. *Mod. Pathol.* 19: 34–48.
48. Chirieac, L. R., G. S. Pinkus, J. L. Pinkus, J. Godleski, D. J. Sugarbaker, and J. M. Corson. 2011. The immunohistochemical characterization of sarcomatoid malignant mesothelioma of the pleura. *Am. J. Cancer Res.* 1: 14–24.
49. Yaziji, H., H. Battifora, T. S. Barry, H. C. Hwang, C. E. Bacchi, M. W. McIntosh, S. J. Kussick, and A. M. Gown. 2006. Evaluation of 12 antibodies for distinguishing epithelioid mesothelioma from adenocarcinoma: identification of a three-antibody immunohistochemical panel with maximal sensitivity and specificity. *Mod. Pathol.* 19: 514–523.
50. Raica, M., A. M. Cimpean, and D. Ribatti. 2008. The role of podoplanin in tumor progression and metastasis. *Anticancer Res.* 28: 2997–3006.
51. Bergman, I., P. H. Basse, M. A. Barmada, J. A. Griffin, and N. K. Cheung. 2000. Comparison of in vitro antibody-targeted cytotoxicity using mouse, rat and human effectors. *Cancer Immunol. Immunother.* 49: 259–266.
52. Caragine, T. A., M. Imai, A. B. Frey, and S. Tomlinson. 2002. Expression of rat complement control protein Crry on tumor cells inhibits rat natural killer cell-mediated cytotoxicity. *Blood* 100: 3304–3310.
53. Rudnick, S. I., J. Lou, C. C. Shaller, Y. Tang, A. J. Klein-Szanto, L. M. Weiner, J. D. Marks, and G. P. Adams. 2011. Influence of affinity and antigen internalization on the uptake and penetration of Anti-HER2 antibodies in solid tumors. *Cancer Res.* 71: 2250–2259.

Identification of pregnancy-associated plasma protein A as a migration-promoting gene in malignant pleural mesothelioma cells: a potential therapeutic target.

Jun Huang[1], Sho Tabata[1], Soji Kakiuchi[1], Trung The Van[1], Hisatsugu Goto[1], Masaki Hanibuchi[1], Yasuhiko Nishioka[1]

[1] Department of Respiratory Medicine and Rheumatology, Institute of Health Biosciences, The University of Tokushima Graduate School, Tokushima, Japan

Correspondence to: Yasuhiko Nishioka, email: yasuhiko@clin.med.tokushima-u.ac.jp

Keywords: malignant pleural mesothelioma, pregnancy-associated plasma protein A, migration, orthotopic xenograft mouse model

Received: June 30, 2013 *Accepted*: July 6, 2013 *Published*: July 8, 2013

ABSTRACT:

Despite recent advances in treatment, malignant pleural mesothelioma (MPM) remains a deadly disease. Targeted therapy generated broad interests and is highly expected for the treatment of MPM, yet promising preclinical results have not been translated into substantial clinical benefits for the patients. In this study, we tried to identify the genes which play functional roles in cell migration as well as to test whether they can be used as novel targets for molecular targeted therapy for MPM in preclinical model. In our study, pregnancy-associated plasma protein A (*PAPPA*) was identified as a gene whose expression level is correlated with MPM cell migration by correlation analysis combining MPM cell migration ability and their gene expression profiles. Highly migratory cells were selected from MPM cell lines, MSTO-211H, NCI-H290 and EHMES-1 *in vitro* and up-regulation of *PAPPA* in these cells were confirmed. *In vitro*, PAPPA was demonstrated to stimulate the MPM cell migration via cleavage of insulin-like growth factor-binding protein-4 and subsequent release of IGF-1. Gene silencing of *PAPPA* in MPM cells led to reduced migration, invasion and proliferation. Furthermore, *PAPPA* shRNA transfected NCI-H290 when orthotopically inoculated into pleural cavity of severe combined immunodeficiency recipient mice, failed to develop tumors and produce bloody pleural effusion as control shRNA transfected cells did. Our study suggests that *PAPPA* plays a functional role in promoting MPM cell migration and it might serve as a potential therapeutic target for the treatment of MPM.

INTRODUCTION

Malignant pleural mesothelioma (MPM), the most common mesothelioma, is an aggressive tumor associated with prior asbestos exposures that arise from mesothelial surface of pleura [1]. Despite recent advances in treatment, MPM remains a deadly disease. The benefit from surgery is confined to a minority of patients. In addition, cytotoxic chemotherapeutic drugs improve quality of life for unresectable patients, and can prolong survival, though only by a few months at best [2]. There has been substantial interest in the role of targeted agents in the treatment of MPM, a variety of them has been tested as therapy for this malignancy in preclinical studies [3-5], yet promising preclinical data has not been translated into clinical benefits in a significant way [6]. More about the biology of this disease might be needed for the molecular targeted therapy to yield promising new treatment options.

Even though metastases are rarely the cause of death of MPM patients, the unique clinical feature of local spread along tissue planes not only causes increasing pain and functional abnormalities, but also makes it a difficult neoplasm to manage [1, 7]. Cell migration as a key to local invasion, might provide an opening for therapeutic approaches if we can understand more about the molecular biology that underlie it [8]. The goal of our study was

to identify the genes which might be involved in the regulation of cell migration as well as to evaluate whether they can be used as targets for the inhibition of MPM cell migration, invasion or even tumor progression.

To achieve this goal, we investigated the migration ability of 8 human MPM cell lines *in vitro* and their gene expression profiles. Genes whose expressions correlated with cell migration were identified by correlation analysis combining the migration ability of MPM cells and their gene expression profiles. Among these genes, pregnancy-associated plasma protein A (*PAPPA*) caught our attention. *PAPPA*, one of four proteins of placental origin found circulating at high concentrations in pregnant women [9], is now basically recognized as a local regulator of Insulin-like growth factor 1 (IGF-1) bioavailability through cleavage of IGF-binding proteins (IGFBPs) [10-12]. The IGF axis was reported to be involved in the pathogenesis of many cancer types [13], including MPM [14-16], and therapeutics aimed at the IGF axis are under extensive clinical investigation [17]. Accumulating preclinical evidences support the idea that *PAPPA* may play a role in cancer [18-22].

In the present study, a series of *in vitro* assay was performed to try to reveal the mechanism of the migration-promoting role of *PAPPA*. To further confirm the causal role of *PAPPA* in MPM cell migration, we applied both small interfering RNA (siRNA) and small hairpin RNA (shRNA) targeting *PAPPA* to investigate the silencing effects of *PAPPA* on MPM cell migration. Finally, we used an orthotopic xenograft mouse model of MPM [3-5, 24] to evaluate the efficacy of *PAPPA* silencing on tumor development and progression *in vivo*.

RESULTS

Expression of PAPPA is correlated with migration ability in MPM cell lines

To identify potential candidate genes whose function are related with MPM cell migration, we determined the migration ability of eight MPM cell lines using transwell chamber migration assay (Fig. 1A), and obtained their gene expression profiles using Affymetrix whole-genome oligonucleotide microarray (Supplementary Fig. 1A). After we applied Pearson's correlation by combining the migration ability of MPM cell lines and their gene expression profiles, expression levels of several genes revealed relatively high correlations with MPM cell migration ability (Supplementary Fig. 1B). Among these genes, we focused on *PAPPA*, which encodes a secreted metalloproteinase that degrades inhibitory IGFBPs. We validated our microarray expression data for *PAPPA* with quantitative real time PCR (qRT-PCR) (Fig. 1B). Overall, *PAPPA* expression results generated from the two different techniques were well correlated (Supplementary Fig. 1B), except that of NCI-H28. Thus we did not include NCI-H28 in the following studies. The similarity of expression levels of *PAPPA* obtained from microarray and qRT-PCR can also be extended to their correlations with MPM cell migration ability (Supplementary Fig. 1B, Fig. 1C). Considering that PAPPA functions as a secreted protein, we further determined the secreted protein levels of PAPPA in the conditioned medium (48 h) of MPM cell culture (Fig. 1D). The secreted PAPPA levels of MPM cell lines are also tend to be positively correlated with their migration ability (Fig. 1E, Pearson $r = 0.7217$, $P = 0.0671$).

Considering the possibility that the correlation is simply due to coincidence, rather than the functional role of *PAPPA* in the regulation of MPM cell migration, we applied an *in vitro* selection strategy to further examine this correlation (Fig. 2A). Highly migratory MPM cells were selected, and their gene expression levels were examined. Three MPM cell lines, MSTO-211H, NCI-H290 and Y-MESO-14, after 3-5 round *in vitro* selection, increased their migration ability roughly 5-fold compared to their corresponding parental cell lines (Fig. 2B). Interestingly, when analyzing their gene expression profiles with microarray, we found that the genes including *PAPPA*, which we previously identified whose expression levels were positively correlated with migration ability (Supplementary Fig. 1B), were also expressed moderately higher in selected highly migratory cells as compared with their parental cell lines (Supplementary Table 1, Supplementary Fig. 3). Increased expression of *PAPPA* in highly migratory cells was further validated by qRT-PCR (Fig. 2C). These observations strongly indicated that there is an inherent relationship between *PAPPA* expression and migration ability in MPM cells.

Major components of the IGF system are expressed in MPM cell lines

PAPPA has long been identified as a local regulator of IGF bioavailability through cleavage of IGFBP4 [10-12], while IGF-1 has already been reported that it can induce MPM cell migration, a biological effect associated with IRS-2 phosphorylation [15]. We speculated that *PAPPA* may play a functional role in regulation of migration of MPM cells, at least partially, through the IGFBP-4/IGF-1/IGF-1R1 axis. Thus we characterized the major components of the IGF axis in MPM cell lines we used. IGF-1R expressions were detected at both mRNA and protein levels (Fig. 3A, 3B), which is consistent with previous report [23]. For IGF-1, no significant levels of secreted IGF-1 were detected by ELISA, and actually no mRNA of *IGF1* was detected by qRT-PCR (data not shown). For IGFBPs, we examined the mRNA transcript profiles of *IGFBP1* to *5* of MPM cells, notably,

IGFBP3 and *IGFBP4* were found to be the dominant IGF-1 binding proteins (Fig. 3C) expressed in MPM cell lines. We subsequently measured the concentrations of secreted IGFBP-3 (Fig. 3D) and IGFBP-4 (Fig. 3E) in the conditioned medium of MPM cell cultures. To test whether the PAPPA detected in the MPM cell conditioned medium is enzymatically active, we incubated rhIGFBP-4, rhIGF-1 with conditioned medium for 24 h, and subjected the conditioned medium to immunoblotting analysis. The conditioned medium of MPM cells did reveal enzymatic activity, as indicated by reduced rhIGFBP-4 after incubation (Fig. 3F). And the enzymatic activity of the conditioned medium seems to be correlated with the concentrations of PAPPA in these medium (Fig. 3F, Fig. 1D). Since tissue plasminogen activator (tPA) was reported to have IGFBP-3 proteolytic activity [24], and we also detected that PLAT (gene encoding tPA protein) is expressed in MPM cell lines (Supplementary Fig. 1B), we performed an *in vitro* proteolysis analysis to see whether the enzymatic cleavage of IGFBP-4 of conditioned medium of MPM cells can also be attributed to tPA. It turned out that PAPPA revealed proteolytic activity of IGFBP-4 but not IGFBP-3, while tPA revealed proteolytic activity of IGFBP-3 but not IGFBP-4 (Fig. 3G), supporting the idea that PAPPA is specifically responsible for the IGFBP-4 proleolytic activity of MPM cell conditioned medium. Taken together, the major components of the IGF axis are expressed in MPM cells, which gives the context of functional role of PAPPA as local regulator of IGF-1 for MPM cells.

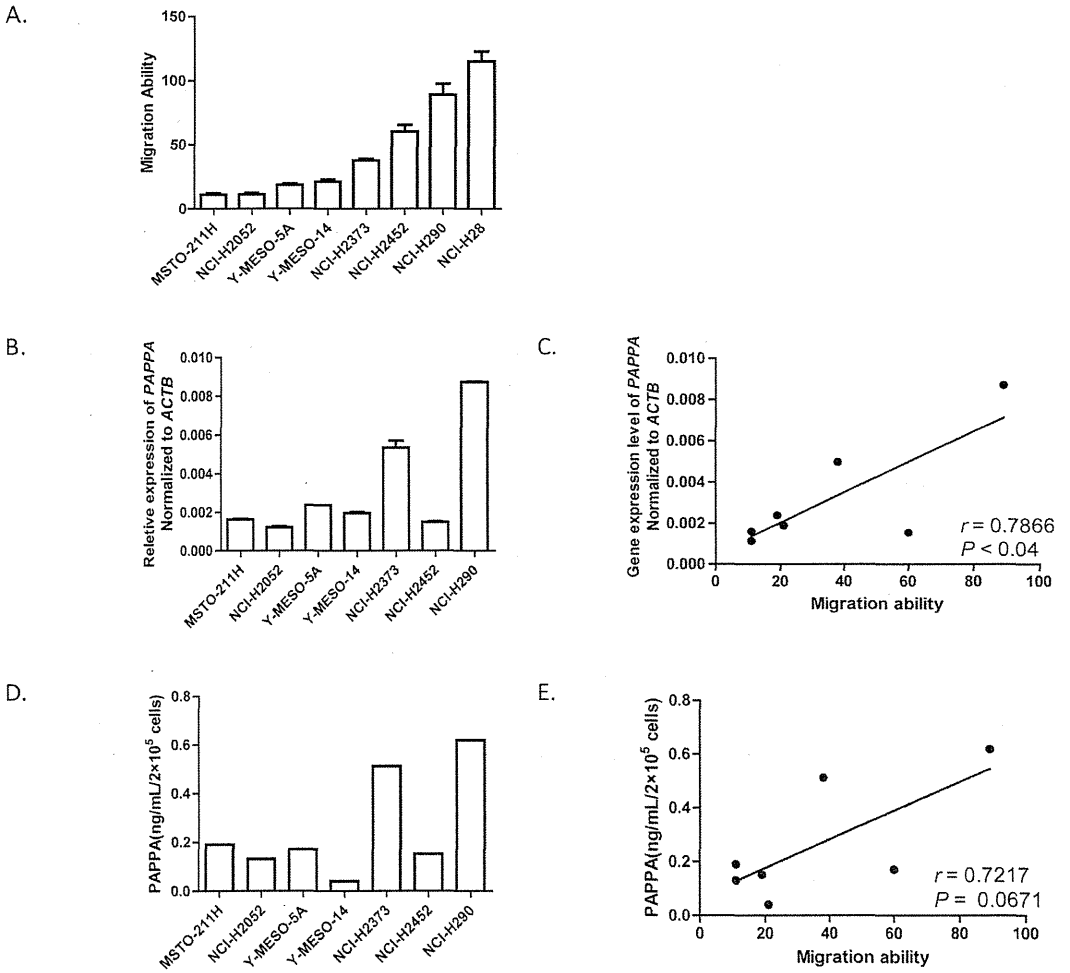

Figure 1: Migration abilities of malignant pleural mesothelioma cells are positively correlated with their expression levels of PAPPA. A, The migration abilities of eight MPM cell lines determined by transwell migration assay, data are the means ± SEMs of three independent experiments. B, The expression levels of *PAPPA* in eight MPM cell lines determined by qRT-PCR. Data are representative of two independent assays carried out in triplicate (means ± SDs, n=3). C, The expression levels of *PAPPA* in eight MPM cell lines determined by qRT-PCR, were positively correlated with their migration ability. * $P<0.05$. The correlation efficient (r) and the significance (P) were calculated by Pearson's correlation analysis. D, The concentrations of secreted PAPPA in the conditioned medium (48 h) were determined by ELISA. E, The concentrations of secreted PAPPA from MPM cells (D) tend to have positive correlation with their migration abilities. $P=0.0671$. The correlation efficient (r) and the significance (P) were calculated by Pearson's correlation analysis.

PAPPA enhanced migration of MPM cells by enzymatically cleaving inhibitive IGFBP-4 and releasing IGF-1 as chemotactic factor

To test the hypothesis that PAPPA could affect MPM cell migration via IGFBP-4/IGF-1/IGF-1R axis, a series of experiments were performed using transwell chamber assays with related recombinant proteins. Consistent with previous reports [15, 25], IGF-1 alone could stimulate the migration of EHMES-1 and MSTO-211H cells across a porous membrane in a dose-dependent manner (Fig. 4A, Fig. 4C). We also demonstrated that stimulating effect of IGF-1 could be blocked by IGFBP-4, while further addition of PAPPA would recover the stimulating effects of IGF-1 on MPM cell migration (Fig. 4B, Fig. 4D). PAPPA alone added to the lower chamber has no effects on cell migration (data not shown), excluding the possibility that the enhanced migration of MPM was due to the direct chemotactic effect of PAPPA. To further confirm that the released IGF-1, rather than the fragments of IGFBP-4 generated by cleavage, recovered the enhanced cell migration, anti-IGF-1 antibody was used to neutralize the released IGF-1 from IGFBP-4 proteolysis caused by PAPPA. The enhanced cell migration was completely abrogated by anti-IGF-1 antibody (Fig. 4E). Taken together, our results suggest that PAPPA could enhance the migration of MPM cell via proteolysis of IGFBP-4 and subsequently releasing IGF-1 as chemotactic factor.

Silencing PAPPA by small interfering RNA inhibited migration and proliferation of MPM cells

To investigate the function of endogenous *PAPPA* on MPM cell migration more directly, we knocked down *PAPPA* in MPM cells (NCI-H290, MSTO-211H and EHMES-1) using siRNA and subsequently evaluated their migration ability. Efficacy of *PAPPA* silencing by siRNA were confirmed by qRT-PCR before the following functional assays (Fig. 5A). We found that *PAPPA* silencing significantly reduced cell migration (Fig. 5B). No difference of cell viability was observed at the time point of migration (24-30 h after siRNA treatment), as revealed by MTT assay (data not shown), but the inhibition of cell growth was also observed later, which became evident 72 h after *PAPPA* siRNA treatment (Fig.

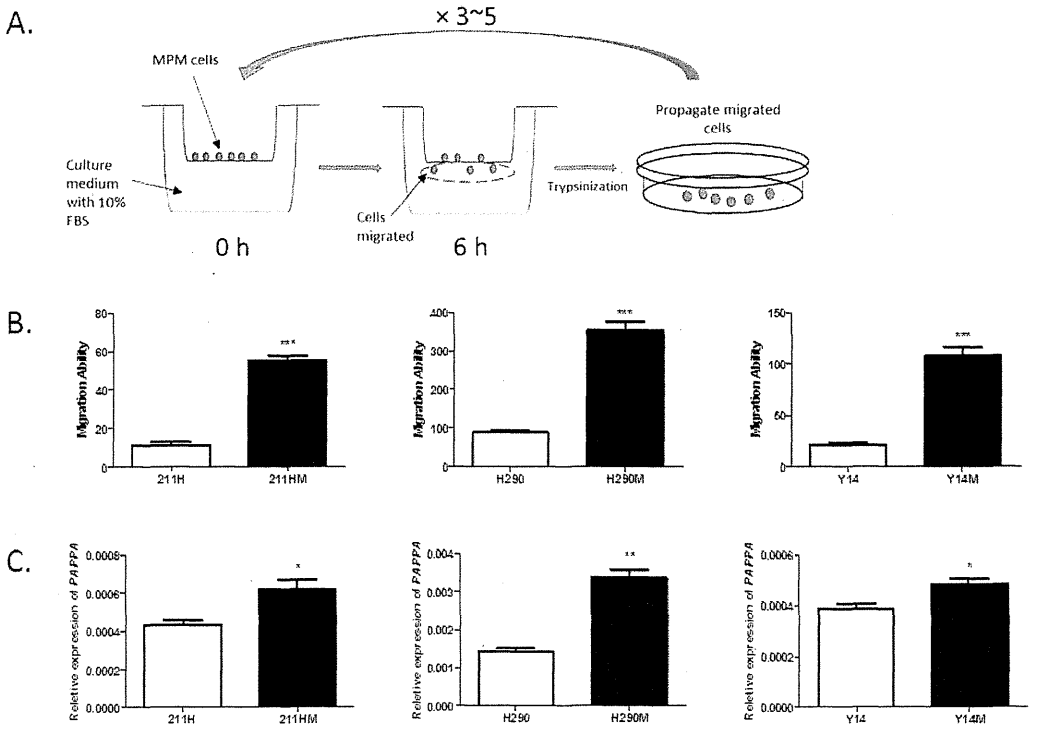

Figure 2: Selected highly migratory MPM cells and their PAPPA expression levels. A, Schematic representation of *in vitro* selection of highly migratory cells. B, The cells that went through *in vitro* selection process revealed higher migration ability (means ± SDs, n=3). Left, NCI-211H parental cell (211H) versus NCI-211 highly migratory cells (211HM). *** $P<0.001$, unpaired *t* test; middle, NCI-H290 parental cell (H290) versus NCI-H290 highly migratory cells (H290M). *** $P<0.001$, unpaired *t* test; right, Y-MESO-14 parental cells (Y14) versus Y-MESO-14 highly migratory cells (Y14M). *** $P<0.001$, unpaired *t* test. C, The expression levels of *PAPPA* in selected cells were significantly higher as compared with that in parental cells. The data are representative of two independent assays carried out in triplicate (means ± SDs, n=3). Left, 211H versus 211HM. * $P<0.05$, unpaired *t* test; middle, H290 versus H290M, * $P<0.05$, unpaired *t* test; right, Y14 versus Y14M, * $P<0.05$, unpaired *t* test.

5C). These data confirmed the functional roles of *PAPPA* on the migration of MPM cells and revealed an extended role of *PAPPA* on the proliferation of these cells, indicating it might be directly used as therapeutic target to inhibit progression of MPM *in vivo*.

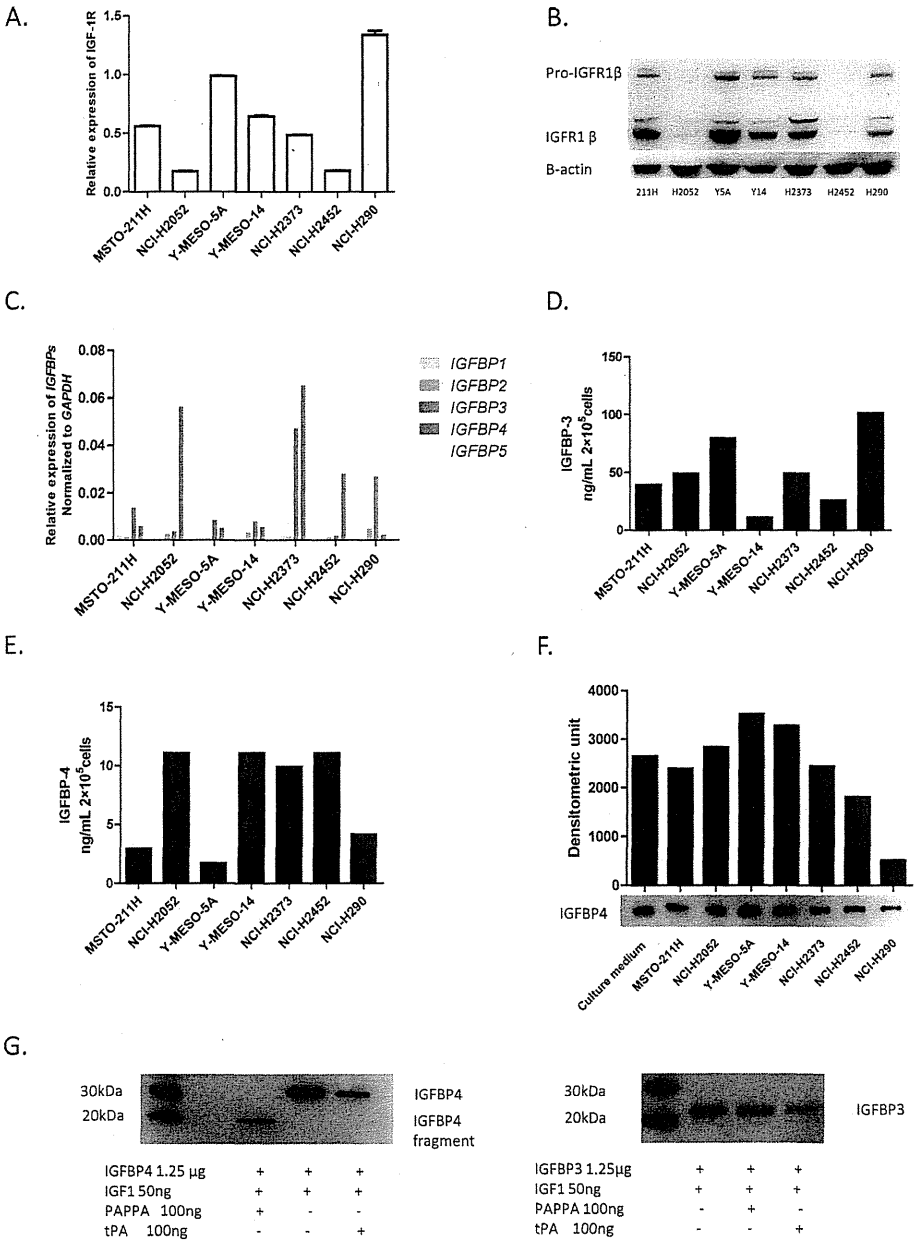

Figure 3: Characterization of major IGF components expression in MPM cell lines. A, Relative gene expression levels of IGF-1R in MPM cell lines assessed by qRT-PCR, normalized to the relative expression of IGF-1R in Y-MESO-5A cells. The data are representative of two independent assays carried out in triplicate (means ± SDs, n=3). B, IGF-1R1 expression detected by immunoblotting. C, Relative gene expression levels of *IGFBP*s in MPM cell lines characterized by qRT-PCR, normalized to that of *ACTB*. D, The concentrations of secreted IGFBP-3 in the conditioned medium (24 h) of MPM cells detected by ELISA. E, The concentrations of secreted IGFBP-4 in the conditioned medium (24 h) of MPM cells by ELISA. F, The conditioned medium of MPM cell lines revealed enzymatic activity of cleaving IGFBP-4. For the detection of IGFBP-4 proteolysis, rhIGFBP-4 (0.5 µg), rhIGF-1 (100 ng) were add into 50 µl conditioned medium of MPM cells and incubated for overnight at 37°C, then conditioned medium was subjected to immunoblotting analysis. G, The enzymatic activity of conditioned medium of mesothelioma cell lines. Left panel, rhIGF-1, rhIGFPB-4 was incubated with or without rhPAPPA for 24 h, and then subjected to immunoblotting analysis. rhPAPPA but not rhtPA revealed specific enzymatic activity of cleavage of IGFBP4. Right panel, rhtPA specifically cleaved rhIGFBP-3.

Transfection of PAPPA shRNA inhibited migration, invasion and proliferation of NCI-H290 cell line in vitro and tumor growth in orthotopic xenograft model

Our next series of experiments were aimed at further determining the phenotypic effects on MPM cells from *PAPPA* knockdown by establishing stable *PAPPA* knockdown cell lines. To establish stable cell line, we chose MPM cell line NCI-H290, which can be used to establish an orthotopic xenograft model of human MPM. This model reflects the clinical features of MPM patients, such as local tumor progression, malignant bloody pleural effusion in the pleural cavity [3-5, 26]. Silencing of *PAPPA* expression in cells transfected with *PAPPA* shRNA was confirmed (Fig. 6A) before carrying out following assays. Consistent with the results of transient knockdown of

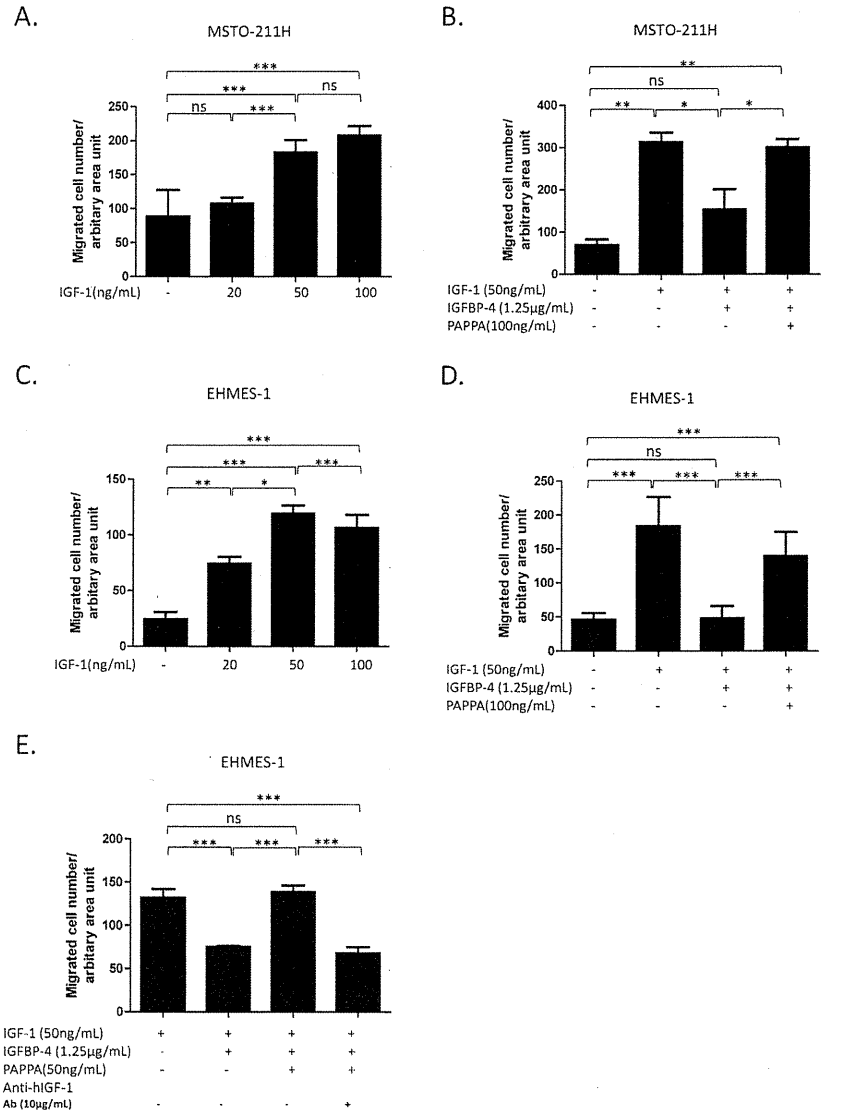

Figure 4: PAPPA enhances migration of MPM cells by enzymatically cleaving inhibitive IGFBP-4 and releasing IGF-1 as chemotactic factor. A, rhIGF-1 induced migration of MSTO-211H cells in a dose-dependent manner. B, rhIGFBP-4 inhibited migration of MSTO-211H cells induced by rhIGF-1, while rhPAPPA recovered the ability of rhIGF-1 to induce migration of MSTO-211H. rhIGF-1 or rhIGF-1 + rhIGFBP-4 or rhIGF-1 + rhIGFBP4 + rhPAPPA were added in serum free medium and incubated at 37°C for 6 h before added into the lower chamber. C, rhIGF-1 attracted EHMES-1 cells to migrate dose-dependently. D, rhPAPPA recovered the ability of rhIGF-1 to induce the migration of EHMES-1 which was inhibited by rhIGFBP-4. E, An anti-IGF-1 antibody blocked the reversing effect of rhPAPPA on the migration of EHMES-1. Six-hours after the incubation with the rhIGF-1, rhIGFBP-4 and rhPAPPA mixture, an anti-IGF-1 antibody was added into the mixture and incubated for another 30 min before being added into the lower chambers. The data are representative of at least two independent assays carried out in triplicate (means ± SDs, n=3).* $P<0.05$, ** $P<0.01$, *** $P<0.001$, ns=not significant, one way ANOVA analysis.

PAPPA by siRNA, migration ability of *PAPPA* shRNA cells was substantially reduced as compared to that of control shRNA cells (Fig. 6B). We also assessed the invasiveness of *PAPPA* shRNA cells using a Matrigel-coated transwell invasion assay. The decrease of invasiveness of *PAPPA* shRNA cells until 20-30% was even more profound than that of their migratory motility until 30-40% as compared to control shRNA cells (Fig. 6B, Fig. 6C). Also consistent with siRNA experiments, we observed a retardation of proliferation of *PAPPA* shRNA cells *in vitro*, as revealed by MTT assay (Fig. 6D). Despite of the growth retardation observed, the cells seem to be viable for a long time (for at least 14 days we followed) as assessed by morphological observation and Trypan blue exclusion test (data not shown).

Finally, we used a mouse orthotopic xenograft model to investigate the roles of *PAPPA* in MPM tumor progression *in vivo*. NCI-H290 cells stably transduced with *PAPPA* shRNA or control shRNA were orthotopically implanted into the pleural cavity of SCID mice. Mice were sacrificed 21-23 days after tumor cell inoculation. Control shRNA NCI-H290 developed tumors in the pleural cavity in all recipient mice at the time point of sacrifice, and showed classical patterns of diffusely grown pleural-based masses. Four out of five mice developed bloody pleural effusions (hemothorax). On the other hand, *PAPPA* shRNA NCI-H290 only developed traces of tumor mass, and almost no pleural effusions were observed (Fig. 6E, Fig. 6F). Taken together, transfection of *PAPPA* shRNA in MPM cells confirmed the important role of *PAPPA* in cell migration, invasion and proliferation, further revealed its crucial role in MPM tumor development and progression *in vivo*.

DISCUSSION

In this study, we identified *PAPPA* as a migration-promoting gene in MPM cell lines. By applying a novel approach of combination of transwell migration assay and microarray gene expression profiling, expression level of *PAPPA* is found to be correlated with migration ability of MPM cell lines. The correlation between *PAPPA* expression and migration ability in MPM was further supported by an *in vitro* selection strategy. *PAPPA* expression was found to be parallelly up-regulated in three migratory cell lines as compared to their corresponding parental cell lines. These results strongly suggested that *PAPPA* functionally promotes MPM cell migration.

The role of PAPPA as a local regulator of IGF bioavailability through cleavage of IGFBPs has been well documented [10-12], and the IGF axis was identified as one of the molecular networks involved in the formation,

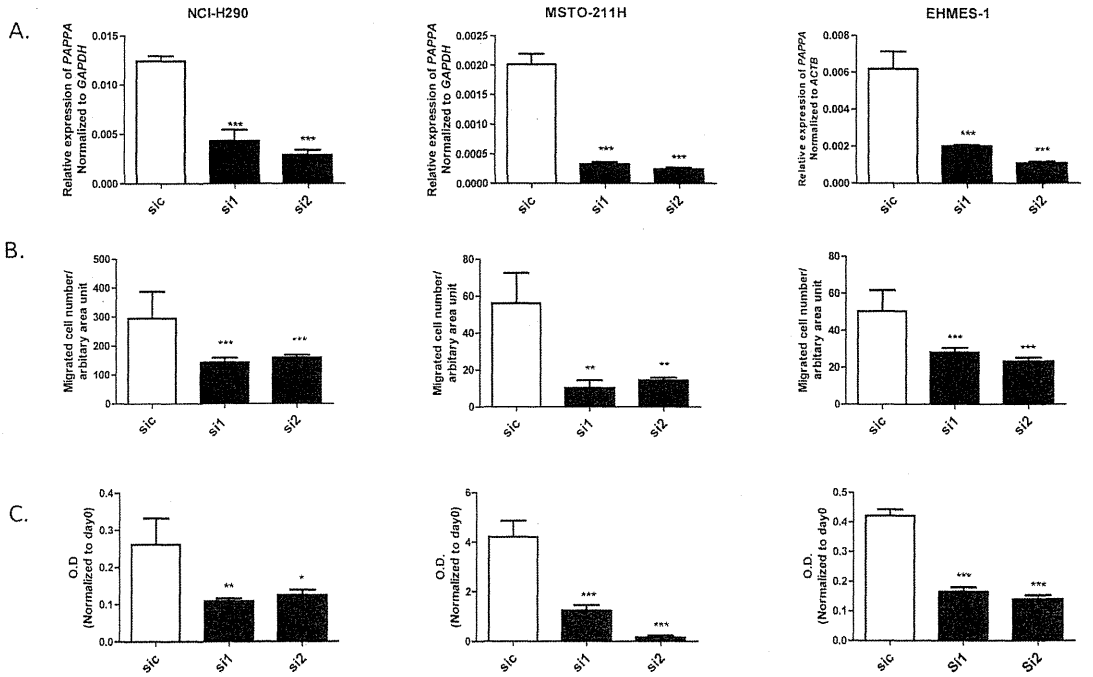

Figure 5: Effects of knockdown of PAPPA by siRNA on migration and proliferation of MPM cells. A, The expression of *PAPPA* in MPM cells (left, NCI-H290; middle, MSTO-211H; right, EHMES-1) was analyzed by qRT-PCR 24 h after transfection with siRNA targeting *PAPPA*. B, The migration ability of MPM cells (left, NCI-H290; middle, MSTO-211H; right, EHMES-1) were determined by transwell migration assay 24 h after transfection with siRNA targeting *PAPPA*. C, The proliferation of MPM cells (left, NCI-H290; middle, MSTO-211H; right, EHMES-1) was determined by MTT assay 72 h after transfection with siRNA targeting *PAPPA*. The data are representative of two independent assays carried out in triplicate (means ± SDs, n=3), * $P<0.05$, ** $P<0.01$, *** $P<0.001$, one way ANOVA analysis.

progression and metastatic spread of many cancer types [13], including MPM [14-16, 27]. Based on this observation, we speculated that PAPPA could promote MPM cell migration via IGF-1. To set the stage for the functional role of *PAPPA*, we characterized the major components of the IGF axis in MPM cell lines. IGF-1R and IGFBP1-5 were found to be expressed at varied levels in MPM cell lines. Our further experiments clearly demonstrated that the migration-promoting role can be explained by, at least partly, its proteolytic activity of IGFBP-4 to regulate the bioavailability of IGF-1. Previous studies showed the overexpression of IGF-1 in both MPM cell lines and tissues versus nonmalignant mesothelium at transcriptional level [14, 15], but we did not detected significant expression of IGF-1 at transcriptional level, which was consistent with another large-scale transcriptional profiling study of MPM [28]. The reason for this discrepancy among different reports remains to be determined, which might be explained by the variety of samples investigated. Despite of the discrepancy, given the fact that physiological ranges of serum IGF-1 concentration [29] by far exceed the concentration of IGF-1 needed to have effects on MPM cell migration as demonstrated by us and others [15, 25], we believe that

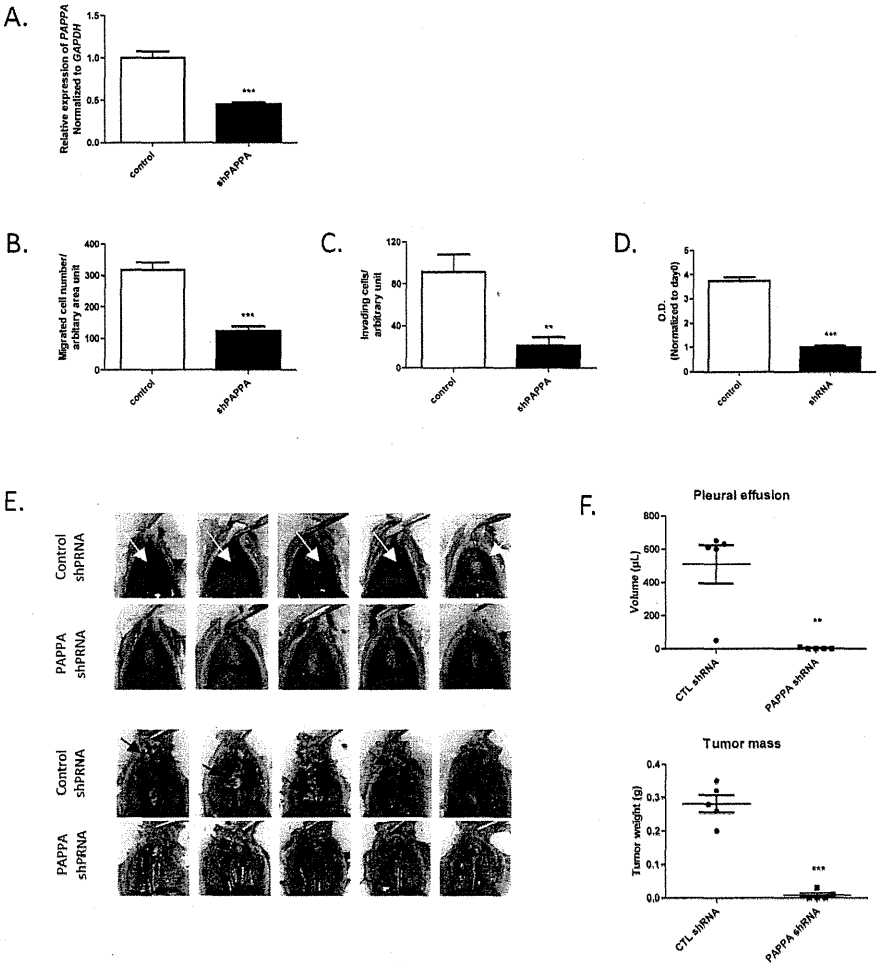

Figure 6: Effects of PAPPA shRNA transfection on migration, invasion, proliferation of NCI-H290 in vitro and tumor growth in orthotopic xenograft model. A, After transfection of *PAPPA* shRNA, gene silencing efficacy of *PAPPA* shRNA in NCI-H290 was confirmed by qRT-PCR. *** $P<0.001$, unpaired *t* test. B, The migration ability of NCI-H290 cells transfected with *PAPPA* shRNA was significantly reduced as compared to that of cells transfected with nonsilencing control shRNA. The data are representative of two independent assays carried out in triplicate (means ± SDs, n=3), *** $P<0.001$, unpaired *t* test. C, The cell invasion through the Matrigel was significantly less in *PAPPA* shPAPPA transfected NCI-H290 cells as compared to that in cell transfected with control shRNA. The data are representative of two independent assays carried out in triplicate (means ± SDs, n=3), *** $P<0.001$, unpaired *t* test. D, The proliferation of *PAPPA* shRNA transfected cells was inhibited as compared to that of cells transfected with control shRNA. The data are representative of two independent assays carried out in triplicate (means ± SDs, n=3), *** $P<0.001$, unpaired *t* test. E, The effects of *PAPPA* shRNA on MPM tumor progression in the SCID mouse model of orthotopic xenograft. Pictures of the gross appearance of bloody pleural effusion (upper panel, white arrow) and tumor mass (lower panel, black arrow) of each group were shown. F, The qualitative analysis of pleural effusion (upper panel, ** $P< 0.01$, unpaired *t* test) and tumor mass (lower panel, *** $P < 0.001$, unpaired *t* test).

our experiments does have its physiological or even pathogenic relevance. It is worth noting that even though PAPPA did enhance MPM cell migration via IGFBP-4/IGF-1 axis in our experimental setup, we did not exhaust the possibility that nonproteolytic mechanisms might be involved in the migration-promoting function of *PAPPA*.

In the present study, the functional role of *PAPPA* in MPM cell migration was investigated by gene silencing experiments using both siRNA and shRNA. Knockdown of *PAPPA* led to reduced MPM cell migration, invasion and proliferation. Exogenously addition of PAPPA could barely rescue the proliferation of MPM cells from the inhibitory effect of PAPPA silencing *in vitro* (data not shown). This implies that PAPPA might involve in an additional mechanism which has yet to be elucidated. In addition, NCI-H290 cells transfected with PAPPA shRNA, when inoculated into the pleural cavity of SCID mice, failed to develop tumors *in vivo*, while NCI-H290 transfected with control shRNA developed massive tumors and bloody pleural effusions. These observations indicate that *PAPPA* facilitates the progression of MPM and that it might be a potential therapeutic target.

Accumulating evidences support the notion that PAPPA may play a role in cancer. *PAPPA* knockout mice were observed to have reduced incidence of spontaneous cancers [18]. A tumor growth-promoting role of *PAPPA* has been demonstrated in breast cancer [20] ovarian cancer [21] and lung cancer [22] with mouse models very recently. Even though the role of *PAPPA* in cancer has not gathered much attention, IGF-1, the pervasive growth factor whose local bioavailability it regulates, has long been an intense interest for cancer researchers [13]. Actually, several novel therapeutics aimed at the IGF-1/IGF-1R, particularly monoclonal antibodies and small molecule tyrosine kinase inhibitors are under clinical investigation [17]. A phase II clinical trial of cixutumumab, a monoclonal antibody to IGF-IR, which showed encouraging therapeutic efficacy for MPM in preclinical study [23], is currently ongoing for the treatment of patients with mesothelioma. Given the vital physiological function of IGF-1 axis, unforeseen enduring effects on metabolism, body fat, muscle mass, and bone density has been major concerns [17]. In contrast to the pervasive existence and versatile physiological functions of IGF-1 axis, *PAPPA* is barely expressed in adult tissues except placenta, cardiamyocyte and smooth muscle [30], and actually genetic deletion of *PAPPA* extended mean and maximum lifespan of by 30-40% in mice [19]. Therefore, *PAPPA* might serve as a better therapeutic target for MPM with more tumor specificity and less risks of side effects as compared to IGF-1 axis components as targets. Even though most of the studies on *PAPPA* so far suggested its tumor-promoting role is largely IGF-1-dependent, anti-*PAPPA* therapy might provide therapeutic effects beyond the inhibition of the IGF-1/IGF-1R signaling axis. A recent study indicated that IGFBP-4 could inhibit angiogenesis both induced by IGF-1 and FGF-2 [31], Therfore, given the fact that the inhibition of PAPPA can lead to the stabilization of IGFBP-4, targeting *PAPPA* might provide extra therapeutic benefits due to angiogenesis inhibition via IGFBP-4/FGF-2 interaction. In addition, there are evidences showing that PAPPA could promote angiogenesis in the chick chorioallantoic membrane assay via a possible nonproteolytic mechanism [32], further supporting the idea that PAPPA is not simply an alternative target for IGF-1 axis, but a novel target might provide extra therapeutic effects. Actually our preliminary data implied that nonproteolytic mechanisms might be involved in the function of PAPPA in MPM cells (data not shown). Now we are trying to validate these preliminary findings and further investigate the mechanistic role of *PAPPA* in the pathogenesis of MPM.

To conclude, our results supported the idea that *PAPPA* can function as a migration-promoting gene in MPM cells, and revealed that its migration-promoting role could be partially explained by its proteolytic activity. Given the fact that knockdown of *PAPPA* affected cell functions including cell migration *in vitro* and tumor development *in vivo*, we propose that it might be used a novel therapeutic target for the treatment of MPM.

METHODS

Cell culture

The human MPM cell lines, MSTO-211H, NCI-H2052, NCI-H2373, NCI-H2452 and NCI-H28, were purchased from the American Type Culture Collection (Manassas, VA). The human MPM cell lines, NCI-H290 and EHMES-1, were kindly provided by Dr. Adi F. Gazdar (University of Texas South-western Medical Center, Dallas, TX) and Dr. Hironobu Hamada (Ehime University, Toon, Japan), respectively. The human MPM cell lines, Y-MESO-14 and Y-MESO-5A, were established as described previously [33]. These MPM cell lines were maintained in RPMI1640 (Nissui Pharmaceutical, Tokyo, Japan) supplemented with 10% heat-inactivated fetal bovine serum (GIBCO, Grand Island, NY), penicillin (100 U/ml), and streptomycin (50 μg/ml). All cell lines were incubated at 37°C in a humidified atmosphere of 5% CO_2. Cell lines were authenticated by DNA fingerprinting [34].

Migration and invasion assay

Cell migration was determined by using 24-well transwell chambers with polycarbonate membranes (8.0-μm pore size; BD Biosciences, Bedford, MA). Human MPM cell suspensions in serum free medium were added to the upper chamber at 1×10^5 cells per well. RPMI-

1640 culture medium with or without 10% FBS were added in the lower well, and the cells were allowed to migrate for 6 h at 37°C in CO_2 incubator. Nonmigrant cells were removed from the upper face of the membrane with a cotton swab. The cells were then fixed and stained with Qiff-Quik Staining Kit (Sysmex, Kobe, Japan). The membranes were excised from the chamber and mounted. The migrant cells attached to the lower face of the membrane were counted. For *in vitro* selection of highly migratory cells, we used a method as descripted previously [35]. Briefly, instead of fixing and staining the migrated cells on the lower face of membrane as a routine process, the migrated cells were detached by trypsin treatment, then collected, cultured and propagated. The propagated cells were again subjected to transwell migration assay, and this process was repeated for 3-5 times. Cell Invasion was determined by using Matrigel-coated transwell chambers (BD Biosciences, Bedford, MA) according to protocols similar to that of migration assay except that allowing the cell to migrate for longer time (18 h).

RNA isolation and quantitative RT-PCR

Total cellular RNAs were isolated using RNeasy Mini Kit (Qiagen, Valencia, CA). After quantification and verification for purity (optical density 260/280 ratios between 1.8 and 2.0) with NanoDrop 1000 (Thermo Scientific, Yokohama, Japan), RNA was reversely transcribed with Takara PCR thermal cycler Dice (Takara Bio, Kyoto, Japan) using High Capacity RNA-to-cDNA Kit (Applied Biosystems, Foster City, CA) following the manufacturer's instruction. Subsequent quantitative RT-PCR was carried out with CFX96 real-time PCR system (Bio-Rad, Hercules, CA) using Applied Biosystems' Taqman gene expression assays for *PAPPA* (Hs01032307_m1), *IGFR1* (Hs00609566_m1), *IGF1* (Hs01547656_m1), *IGFBP1* (Hs00236877_m1), *IGFBP2* (Hs01040719_m1), *IGFBP3* (Hs00365742_g1), *IGFBP4* (Hs01057900_m1), *IGFBP5* (Hs00181213_m1). Samples were normalized to *GAPDH* (Hs99999905_m1) or *ACTB* (Hs99999903_m1) and quantification was determined by using the ΔΔCT method.

Microarray analysis

Total RNA from MPM cells was isolated using an RNeasy Mini kit (QIAGEN, Valencia, CA). RNA quality was first checked for chemical purity using a NanoDrop spectrophotomer (NanoDrop Technologies, Wilmington, DE) and then assessed for RNA integrity using the Bioanalyzer 2100 (Agilent Technologies, Santa Clara, CA, USA). One hundred ng of total RNA was amplified and labeled using the Affymetrix Whole-Transcript (WT) Sense Target Labeling Protocol, and labeled RNA was hybridized to GeneChip Human Gene 1.0 ST Array (Affymetrix, Santa Clara, CA). Data visualization and analysis was performed using GeneSpring GX (Version 12.1) software.

ELISA

The human MPM cells (2×10^5) were cultured in medium described above for 24 h, washed with phosphate buffered saline (PBS), 3 ml of fresh culture medium or serum free culture medium were added. After incubation for 24 or 48 h, the culture media were harvested and centrifuged, and the supernatants were stored at −70°C until analysis. Protein levels in supernatants were quantified by ELISA kit for human IGFBP-3, PAPPA (R&D systems, Minneapolis, MN), IGFBP-4 (Abcam, Cambridge, MA) following the manufacturers' instructions.

Immunoblotting analysis

For the detection of IGFR1 expression in cell lines, the cells were lysed in M-PER (Pierce, Rockford, IL) containing phosphatase and proteinase inhibitor cocktails (Roche, Indianapolis, IN). The concentrations of protein were determined using Bio-Rad Protein Assay Kit (Bio-Rad, Hercules, CA). Blots were incubated with antibodies: IGFR1 (diluted 1:500, 111A9, Cell Signaling, Danvers, MA), β-actin (diluted1:5000, I-19, Santa Cruz Biotechnology, Santa Cruz, CA) overnight. For the detection of IGFBP-4 proteolysis, rhIGF-1, rhIGFBP-4, rhPAPPA and rhtPA (R&D systems, Minneapolis, MN) were incubated at the indicated concentration in 50 mM Tris, 10 mM $CaCl_2$, 150 mM NaCl, pH 7.5 buffer for 6 h or overnight at 37°C. Protein mixture was transferred to iBlot™ gel Tranfer Stacker polyvinylidene difluoride (PVDF) membrane (Invitrogen, Carlsbad, CA) according to manufacturer's instruction, the membranes were incubated at room temperature for 2 h with anti-IGFBP-4 (K13RE) antibody (diluted 1:1000, Santa Cruz Biotechnology, Santa Cruz, CA). All analysis were revealed using the horseradish peroxidase(HRP)-labeled anti-rabbit or anti-mouse antibodies (GE Healthcare, Tokyo, Japan), and visualized using SuperSignal West Femto Maximum Sensitivity Substrate (Thermo Scientific, Yokohama, Japan) with a quantitative imaging system LAS4000Mini (Fujifilm, Tokyo, Japan).

In vitro siRNA transfection

Stealth RNAi™ siRNA for *PAPPA* (HSS107591, HSS181743; Invitrogen, Carlsbad, CA) transfection was conducted with Lipofectamine 2000 (Invitrogen, Carlsbad, CA) following the manufacture's protocol. Gene knock down efficacy was confirmed by qRT-PCR at the time